EMERGENT BEHAVIOR IN COMPLICATED SYSTEMS: TINNITUS, SMARTICLES, AND METRONOMES

A Dissertation
Presented to
The Academic Faculty

By

Zachary Lawrence Jackson

In Partial Fulfillment
Of the Requirements for the Degree
Doctor of Philosophy in Physics

Georgia Institute of Technology
May, 2020

EMERGENT BEHAVIOR IN COMPLICATED SYSTEMS: TINNITUS, SMARTICLES, AND METRONOMES

Kurt Wiesenfeld
School of Physics
Georgia Institute of Technology

Daniel Goldman
School of Physics
Georgia Institute of Technology

Simon Sponberg
School of Physics
Georgia Institute of Technology

Joshua Weitz
School of Biological Sciences
Georgia Institute of Technology

Dana Randall
School of Computer Science
Georgia Institute of Technology

Date Approved: March 27, 2020

This is patently absurd; but whoever wishes to become a philosopher must learn not to be frightened by absurdities.

– Bertrand Russell

To my loving fiancé Kristen and Mai the cat, for supporting me every day even when I was difficult.

ACKNOWLEDGMENTS

First, I would like to thank my advisor Kurt for allowing me to work independently and take my research in my own direction, while still always being available for invaluable guidance when I needed it. He has done an excellent job of letting me work the way I want, while still keeping me for doing something stupid.

Next, I would like to thank Dan for allowing me to work with his group and supplying a steady current of interesting and enthusiastic ideas.

Third, I would like to thank the rest of the members of my committee, Simon Sponberg, Joshua Weitz, and Dana Randall for taking the time and effort to read and digest my work.

Lastly, I want to thank the Georgia Tech School of Physics as a whole for allowing me to attend. I still can't believe you let me in, but I am very glad you did.

TABLE OF CONTENTS

LIST OF TABLES

LIST OF FIGURES

SUMMARY

Patterns of behavior can arise in many body systems that are qualitatively different than that of the individual elements. In this dissertation, we explore emergent behaviors through three different projects. The first is a dynamical model for the inner ear that explores both the onset of tinnitus and the effects of coordinated reset therapy. This non-invasive therapy recently found promising results in a clinical trial. Our model extends an existing theory of individual outer hair cell dynamics to include their mutual interaction, and considers how sustained activity can inhibit the natural recovery exhibited by normal (healthy) individuals. The model is investigated through numerical simulations and shows behavior broadly similar to that reported in the clinical study. Next, we describe the motion of a collection of enclosed "smarticles", small three-link robots which move their arms according to a predetermined gate. Experiments show when all internal smarticles are performing a periodic gate, an enclosing ring can translate, but does not have a preferred direction. It was found that when one smarticle is made inactive and in a straight configuration the collective drifts on average either towards or away from the inactive smarticle, depending on the mass of the enclosing ring. To better understand this biased motion we develop a collision model for the system and then extend that model to include short term correlations to account for fluctuations. Lastly, we identify a class of non-equilibrium systems whose behavior can be described statistically by approximating the some fast varying component of the system as noise. This behavior is demonstrated through a modified Lorenz system as well as a simulation of an array of coupled metronomes. Both examples have the capacity for episodes of distinct behaviors with irregular transitions between them.

Chapter 1
Introduction and Background

1.1 Introduction

There are three projects that make up this dissertation and each constitutes its own chapter. Chapter 2 describes a modeling of tinnitus, with an emphasis on the dynamical and critical behavior of healing and recovery. The goal is to understand the results of a non-invasive therapy that showed some improvement in the condition of patients [1]. With the assertion that the human body is a dynamical system, how would a theory of therapy and healing look from the point of view of a physicist? With the clinical trial in mind we develop a model of the inner ear with extensive biological detail. Then, with healing and recovery in mind we developed a more abstract model of tinnitus-like behavior that retains only the essential elements.

Chapter 3 describes a model for the motion of a constrained swarm robotics system known as a supersmarticle. In experiments, the system exhibits a surprising behavior where the direction and speed of movement changes as a function of the mass of one of the components [2]. How could the motion of a body be redirected by changing an undirected variable of the system? How can we quantitatively model a system of non-conservative components interacting in a highly non-linear way? The result is a coarse graining of the dynamics into a series of stochastic collisions with the resulting displacement from a collision a function of the above-mentioned mass. We then explore the effects of correlations on the system by introducing short time dependence in collision probabilities.

Chapter 4 describes a new class of systems at the interface of deterministic dynamics and statistical mechanics. How do we describe the trajectories of systems where strong fluctuations and deterministic dynamics both play an important role? Can such a system exhibit behavior that is different from either extreme? We examine specific illustrative examples of complicated systems to explore ideas put forward by a recent general treatment of non-equilibrium systems [3]. Through these examples, we explore systems with competition between order and disorder that results in episodes of distinct behavior with irregular duration.

The incepting inspirations for the three projects in this dissertation are very different. One is a medical clinical trial for a new noninvasive tinnitus therapy. Another is experimental results from a robotic active matter system. The last is an abstract and mathematical theory for timescale separated dynamical systems. Nonetheless, a common thread of emergent behavior runs through all three. We mean emergent behavior by the most generous definition: a behavior that arises as a consequence of the interaction between a collection of agents that is qualitatively different than the behavior of any individual actor. In every part of the work in this dissertation we emphasize the importance of coupling and interaction. In the biological system in chapter 2 it is the outer hair cells of the inner ear that mutually excite each other to maintain activity. In the supersmarticle system it is the smarticles who cannot move on their own but diffuse when constrained to interact. The metronomes of section 4.4 exhibit synchronization, maybe the lowest order of emergent behavior, through the motion of a common support.

Another common theme that runs throughout the work described here is the coarse graining of complicated systems. Particularly in the study of an emergent phenomenon, it is often useful to treat a higher-level organization of a system by averaging over a sub-domain or partitioning the state space [4]. This technique is employed in thermodynamics [5], renormalization group theory [6, 7], mean field

theory [8], symbolic dynamics [9], and two-timing [10] . All of these techniques use some averaging to coarse grain a system into macroscopic variables that encode system wide behavior without having to follow the exact dynamics at a microscopic level. In the tinnitus system, we identify macroscopic variables that are a function of averages across the system. In the supermsmarticle system as well as the metronome system we partition the large, high-dimensional state space of the systems into a small group of identified states similar to a symbolic dynamics treatment. By focusing on higher level organization, system wide behavior becomes obvious that could be obscured when studying the full, detailed dynamics.

1.2 Background

In this section we briefly describe two simple examples that demonstrate concepts that are used in a more complicated contexts in later chapters.

1.2.1 Kuramoto Oscillators

The canonical dynamical theory that has been used to model coupled oscillators is the Kuramoto oscillator model[11]. It is a simple all to all coupling model, where each oscillator is given its own natural frequency and coupled to the other members through a sinusoidal function.

$$\dot{\theta}_i = \omega_i + \frac{K}{N}\sum_j \sin(\theta_j - \theta_i), \qquad i \ldots N \tag{1.1}$$

It has been used to describe such diverse living systems as neuron activity in the brain[12, 13], firefly flashes[14], and Josephson junction arrays[15, 16]. A good description of the behavior of this system is given in[17]. Each oscillator has a natural frequency ω_i that it moves with in the absence of the other oscillators. It is influenced by the average of the other members scaled by a coupling constant K characterizing

the strength of the interactions. The ω_i are chosen from a distribution $g(\omega)$ that is taken to be unimodal and symmetric about some frequency Ω. This allows us to shift to a rotating frame where phase locked solutions are stationary.

A useful way to visualize the system is to put the phase of each oscillator on the unit circle and find the centroid (Figure.1.1).

$$re^{i\psi} = \frac{1}{N}\sum_{j}^{N} e^{i\theta_j} \tag{1.2}$$

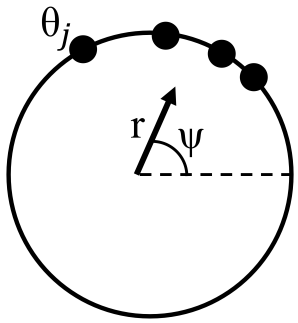

Figure 1.1: **Kuramoto Centroid.** If we place all of the phases on the unit circle and find the centroid then the distance from the center to the centroid gives a natural order parameter.

This formulation gives us an order parameter r that goes from 0 to 1 and measures the level of synchrony of the oscillators. If all the oscillators are phase locked, then $r = 1$ and if all of the phases are equally distributed around the unit circle then $r = 0$. This order parameter can be used to show a transition from an unsynchronized state to a synchronized state as the coupling between the oscillators is increased. Similar order parameters are used in chapters 2 and 4 to characterize the synchrony and activity of other kinds of coupled oscillator systems (Equations.2.8 and 4.13).

This system is a simple example of multiple concepts that are explored through this dissertation. First, the behavior of the system is controlled by the strength of the interactions, and if those interactions are strong enough a new macroscopic behavior

unique to the extended system emerges. Also, the macroscopic state of the system can be characterized by a single order parameter that is a well-chosen average over the individual members.

1.2.2 Two-Timing

A concept that is returned to multiple times throughout this work is a separation of time scales. In the context of the tinnitus model in Chapter 2 and the modified Lorenz equation in Chapter 4 there are some variables that explicitly vary slower than others. One useful way to think about these kinds of systems is described in Ref. [10] called "two-timing". The idea is to split the system into variables that vary slowly and variables that vary quickly and make each subset a function of their own time. An example where this can be described explicitly is the case of a weakly nonlinear van der Pol oscillator.

$$\ddot{x} + x + \epsilon(x^2 - 1)\dot{x} = 0 \tag{1.3}$$

In general, this oscillator has an amplitude and a phase. By treating the slower varying amplitude as a function of "slow time" T and the phase as a function of both T and "fast time" t, we can find the approximate solution.

$$x(t, \epsilon) \approx \frac{2}{\sqrt{1 + 3e^{-\epsilon t}}} \cos(t) \tag{1.4}$$

This solution gives the transient behavior of the system in intermediate time as it approaches the steady state solution by treating the dynamics of the phase and the envelope separately. The exact solution is shown along with the envelope predicted by the two-timing technique in 1.2.

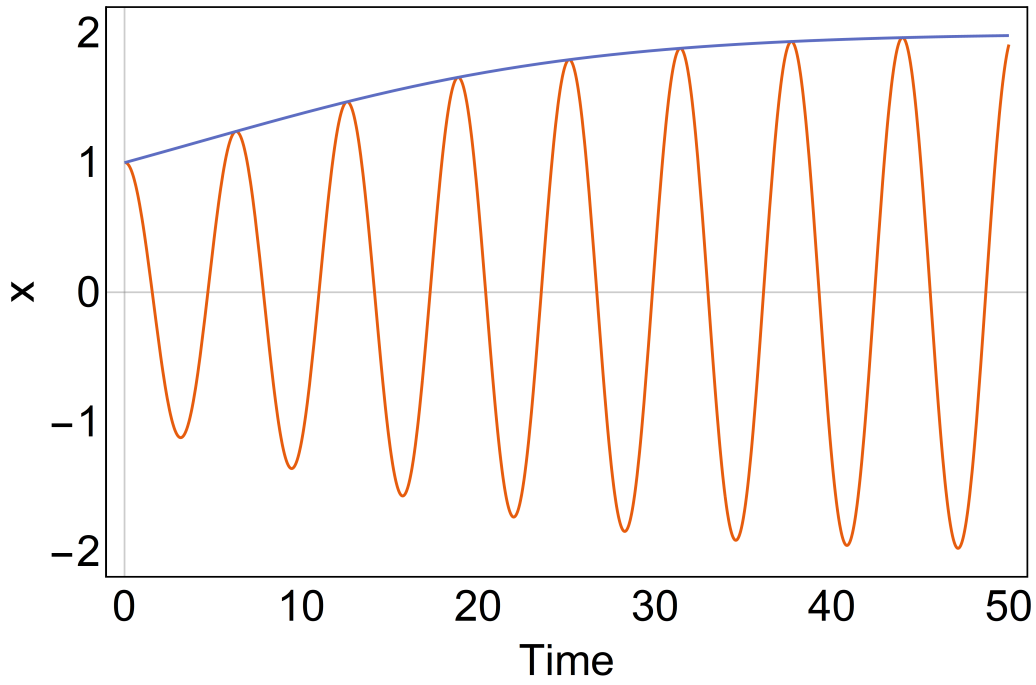

Figure 1.2: **Two timing solution.** Shown is the envelope predicted from the two-timing averageing technique in blue along with the actual solution in orange.

Although things are not always as simple as this explicit case, this kind of approximation is useful to keep in mind when dealing with systems that involve multiple very different time scales. The slower changing variables take more time to react to the effect of the fast variables and so they are approximately reacting to the average of the faster changing variables over some intermediate time.

Chapter 2
Dynamics of Tinnitus and Coordinated Reset Therapy

2.1 Introduction

2.1.1 Dynamical Disease

The systems of the human body exhibit a wide range of typical repeated behavior when they are functioning in a healthy way. This includes the beating of the heart, firing of neurons, circadian rhythm, digestive activity and more. One way to classify the onset of disease is when one of these systems is behaving in an abnormal way with respect to its normal pattern of behavior. From a dynamical systems perspective this means either the trajectory of system has fallen into a new attractor, or the existing attractor has been significantly modified from its healthy state. Modeling bodily processes in this way, and leveraging a dynamical systems perspective to understand and/or treat biological pathologies is known as dynamical disease [18–21].

Treating chronic conditions and injuries in medicine is often a matter of putting the body in a position to heal itself. The symptoms of a condition, such as inflammation, can directly prevent or slow healing, so treating the symptoms can indirectly treat the underlying condition. From the perspective of dynamical systems theory, this situation can be represented as follows. The transition from healthy to unhealthy states may result from a system parameter wandering into an unfavorable range; this situation may persist due to feedback which maintains the parameter in the unhealthy range; suppressing the feedback can allow the parameter to evolve – on a slow time scale – back into a healthy range.

Analogous situations are easy to find. To cite an example from the physical sciences, consider the effect of greenhouse gases on Earth's temperature [22]. The thermodynamic equilibrium between Earth and Sun maintains Earth's temperature in a fairly narrow range. An excess of greenhouse gases results in a temperature rise, but removing the excess might not return temperatures to their original value: a symptom of higher Earth temperatures is icecap melting, which decreases its reflectivity parameter, thereby increasing the rate at which sunlight is absorbed, thus maintaining the warmer temperature. A "therapy" which restored the original (low temperature) reflectivity would allow recovery of the original, colder thermodynamic equilibrium.

In this chapter, motivated by a partially successful clinical trial [1] in which a noninvasive therapy was used to drive the system to a healthier state, we take this dynamical systems view and apply it to tinnitus. Healthy and unhealthy states represent different dynamical attractors; the unhealthy state is maintained even in the absence of external stimulus due to internal feedback; therapy is the application of a particular stimulus which interferes with the harmful feedback, allowing the slow evolution of the system parameters back to a healthy range.

In an effort to understand and reproduce the phenomenology reported in the clinical trials, we present a dynamical model for the inner ear, specifically the organ of Corti. We propose that a gradual wandering of physical parameters in the auditory system can be responsible for the onset of tinnitus in a subset of cases where there is no physical damage. We begin from a model for individual cells introduced by Nadrowski et al. [23], and modify the dynamical equations to include (1) cell-cell interactions induced by the basilar membrane, and (2) very slow parameter evolution associated with common healing. The resulting model broadly reproduces a range of observed behavior: the model allows for states corresponding to healthy activity, transient tinnitus, and sustained tinnitus. In the latter regime, application of a

therapeutic stimulus very similar to that which was used in the clinical trials can result in a substantial reduction in tinnitus activity.

2.1.2 Tinnitus Background

Tinnitus, *i.e.* ringing in the ear, is a problem that affects as much as 15% of the U.S. population [24]. As yet, there is no widely used and effective treatment for the condition [24]. Tinnitus tends to affect older people and people that are relatively over-exposed to loud noises but has a variety of different risk factors and apparent causes [24, 25]. Objective tinnitus, where a physical source for the sound can be identified, is relatively rare and can usually be attributed to abnormal blood flow or muscle contractions [26]. Subjective tinnitus, where the sound is only perceptible to the tinnitus sufferers themselves, is much more common and is more varied in its causes. In a survey of 2000 tinnitus patients 38% of respondents could not identify a particular onset factor, 22% reported prolonged noise exposure and noise trauma, 17% reported head or neck injury, 10% reported infections or neck illness and 13% reported drugs and other medical conditions that corresponded with the onset of their condition [26]. In some cases, there is a clear injury or damage to the physiology of the patient, but in others there is no obvious cause to the onset of tinnitus.

A recent clinical trial reported significant improvement using a non-invasive audio therapy designed to desynchronize the over-active neurons [27]. Motivating the therapy is the theory that synchrony of the neurons in the audio cortex is a cause of the phantom sound [27–30]. The randomized, single blind, placebo-controlled trial involved 63 patients with chronic tonal tinnitus and up to 50 dB hearing loss. Seventy-five percent of the patients reported substantial improvement in their condition according to a post treatment questionnaire. Improvement was widespread but incomplete and symptoms started to return to their previous severity after four weeks without further therapy [1, 28]. This therapy is conceived as a coordinated reset of

audio cortex neurons [27]. Coordinated reset stimulation was initially developed as a deep brain stimulation scheme for long term desynchronization of cerebral neural activity. It was later adapted to an acoustic therapy for tinnitus [27, 31]. Neurological modeling [27] using systems arrays of bursting neurons with excitatory and inhibitory ability as well as plasticity shows a drastic short term effect of therapy (on the order of a few thousand seconds), while the clinical data shows a slower improvement and long term persistence of symptoms [1].

The human ear can detect sounds that are comparable in magnitude to thermal noise [32]. This sensitivity comes from the active amplification of incoming sound. Inside the cochlea, the organ of Corti is responsible for this non-linear amplification. Air vibrations disturb the basilar membrane and those vibrations are relayed to the auditory cortex through the auditory nerve. The mediation between mechanical waves in the membrane and neural activity is performed by hair cells. There are two types of hair cells. The inner hair cells are strongly connected to the brain through the auditory nerve and do most of the signaling to the auditory cortex. The more numerous outer hair cells amplify the sound entering the ear by pushing on the basilar membrane to make quieter sounds easier to perceive and tones easier to distinguish. These cells form rows of three along the basilar membrane. Each cell has a stiff bundle of stereocilia that pivots at the base when disturbed by vibrations in the surrounding fluid and membrane. When the bundle is bent, tension in small links between the stereocilia open gates on the cell that allow the cell to be depolarized and the cell lengthens, pushing on the membrane. The physical arrangement of the hair cells suggests an array of oscillators with local coupling through their common membrane.

2.2 Model

We start with a dynamical model for individual outer hair cells developed by Nadrowski et al. [23], based on the interaction between the motion of a stereocilia bundle and its inter-cilia links. The bundles can be elastically displaced from vertical and the anchor points of the links move to adapt to stress placed on the bundle (see Figure.2.1). The governing differential equations are

$$\lambda \dot{X} = -K_{gs}(X - X_a - DP) - K_{sp}X + F_{ext} \tag{2.1}$$

$$\lambda_a \dot{X}_a = K_{gs}(X - X_a - DP) - \gamma f_{max}(1 - SP) \tag{2.2}$$

$$P = \frac{1}{1 + Ae^{-(X - X_a)/\delta}} \tag{2.3}$$

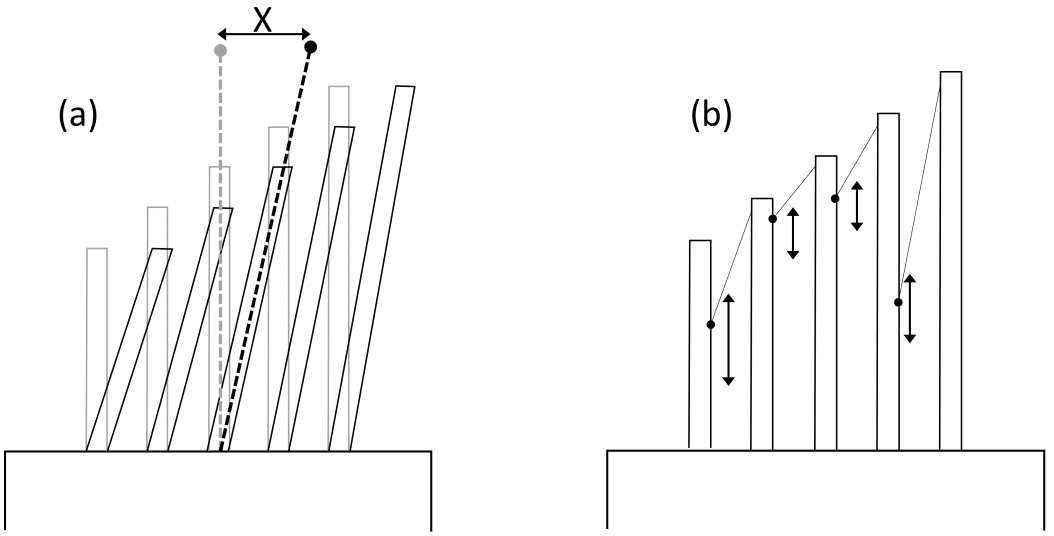

Figure 2.1: **Stereocilia Cartoon.** (a) The stereocilia bundles on the hair cells deflect by a distance X. (b) The stereocilia are attached by tip links that adapt to stress on the cell by translating up or down the anchor cilia. X_a represents the overall configuration of a cells tip link anchors.

where X represents the horizontal displacement of the stereocilia bundle and X_a represents the overall configuration of the anchor points of the inter-cilia links of a

bundle. The first terms for each equation are opposites of each other because the inter-link motors work to minimize the force on the intercilia links by increasing the value of X_a to decrease the value of $K_{gs}(X - X_a - DP)$. The overdot denotes differentiation with respect to time. P is the probability of the gates in a stereocilia bundle to be open and acts as the best measure of the lengthening action of the cell that pushes on the basilar membrane. It is the opening of the gates that allows the depolarization of the cell and the activation of the prestin motor which quickly lengthens the cell to give a "pulse" to the membrane. K_{sp} and K_{gs} are spring stiffness coefficients for the base pivots of the bundles and the gating springs respectively. λ and λ_a characterize the friction in the system. γ is a geometric factor. D is the change in length of the gating spring associated with the opening of a gate. f_{max} is the maximum force that can be exerted by a link. S is a constant that is proportional to the concentration of Ca^{2+} in the fluid surrounding the cell, with higher concentration leading to stronger restoration of the cell to a polarized state. F_{ext} represents the force on the stereocilia bundle from an external source. A and δ account for the energy difference between open and closed states.

In the study of the dynamics of the equations (2.1) - (2.3)[23], it was found that depending on the values of parameters (specifically f_{max} and S), in the absence of external forcing or noise, a hair cell could either be in a state of sustained oscillation or rest. It was also found that with experimentally determined and physically realistic values for the parameters the system operates very close to the critical boundary separating regions of static equilibrium and sustained oscillations.

Now, we go beyond the single hair cell dynamics developed by Nadrowski et al. and we introduce inter-cell interaction through local coupling of the elements. The physical arrangement of the outer hair cells suggests a simple modeling of the full system as a one-dimensional array of elements. We add a coupling term to account for the effect that the outer hair cells have on their neighbors: when a hair cell

lengthens it pushes down on the basilar membrane, causing the stereocilia bundle of its neighbor to deflect away from the activated cell as shown in Figure.2.2. In non-dimensional form, the equations become

$$x_i{}' = -b(x_i - y_i - cP_i) - x_i + \beta_i(P_{i-1} - P_{i+1}) + F_i \tag{2.4}$$

$$y_i{}' = a(b(x_i - y_i - cP_i) - h(1 - SP_i)) \tag{2.5}$$

$$P_i = \frac{1}{1 + AExp[y_i - x_i]} \tag{2.6}$$

where $x_i = \frac{X_i}{\delta}$,$y_i = \frac{X_{ai}}{\delta}$ $c = \frac{d}{\gamma\delta}$, $a = \frac{\lambda}{\lambda_a}$, $b = \frac{k_{gs}}{k_{sp}}$, $h = \frac{\gamma f_{max}}{\delta k_{sp}}$ and primes denote a differentiation with respect to dimensionless time $\tau = \frac{k_{sp}}{\lambda}t$

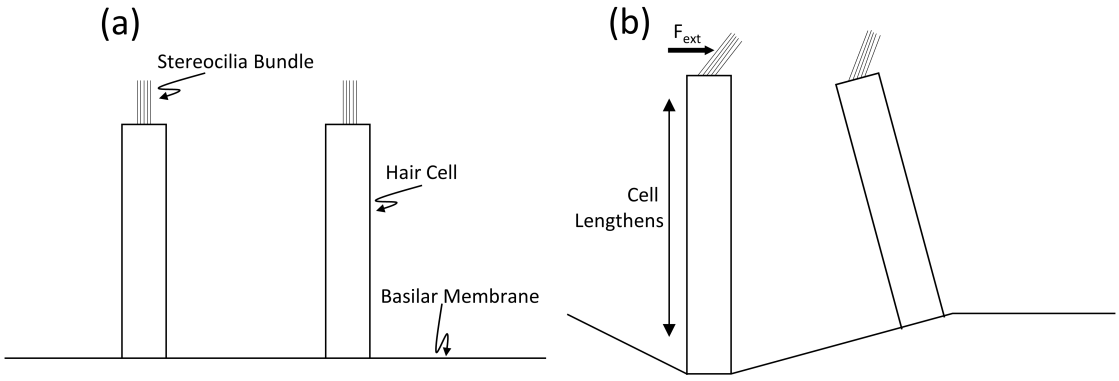

Figure 2.2: **Hair cells and basilar membrane.**(a) Two hair cell elements attached to a common basilar membrane. (b) Coupling between two hair cell elements. The activation of one hair cell causes a disturbance in the stereocilia position of a neighboring cell.

The above-mentioned coupling term appears on the right side of Eq.2.4, with coupling strength controlled by the parameter β.

2.3 Behavior

The model has $2N$ dynamical variables $\{x_i, y_i\}$, and the values of the fixed parameters a, b, c, h, A, S are set using the data reported in Ref.[23]. Note that for this set of parameter values, the single element system has only fixed-point attractors (that is, the system always settles down to a static equilibrium). In what follows, we summarize the behavior of our model, as a function of the new coupling parameter β. In the first set of simulations, we keep β constant, start with a quiescent system, and apply a finite-duration stimulus F_i.

2.3.1 Healthy Behavior

An individual hair cell with healthy parameters values and low coupling reacts to a disturbance with an oscillation during the application of external forcing and then it settles back down to a resting state after a short transient as shown in Figure.2.3. An array of fifteen elements were forced with

$$F_i = 5 \exp\left[-\frac{1}{2}(i-8)^2\right] \sin\left(\frac{2\pi\tau}{i}\right) \tag{2.7}$$

Initially quiescent, the hair cells are forced at different frequencies for a finite time interval (ending at $\tau = 60$). In response, the affected elements oscillate for the duration of the forcing before settling back down to their initial rest state. This reaction is typical of any signal which is short in time. The hair cells are active for the duration of the signal, and then return to a baseline P_i.

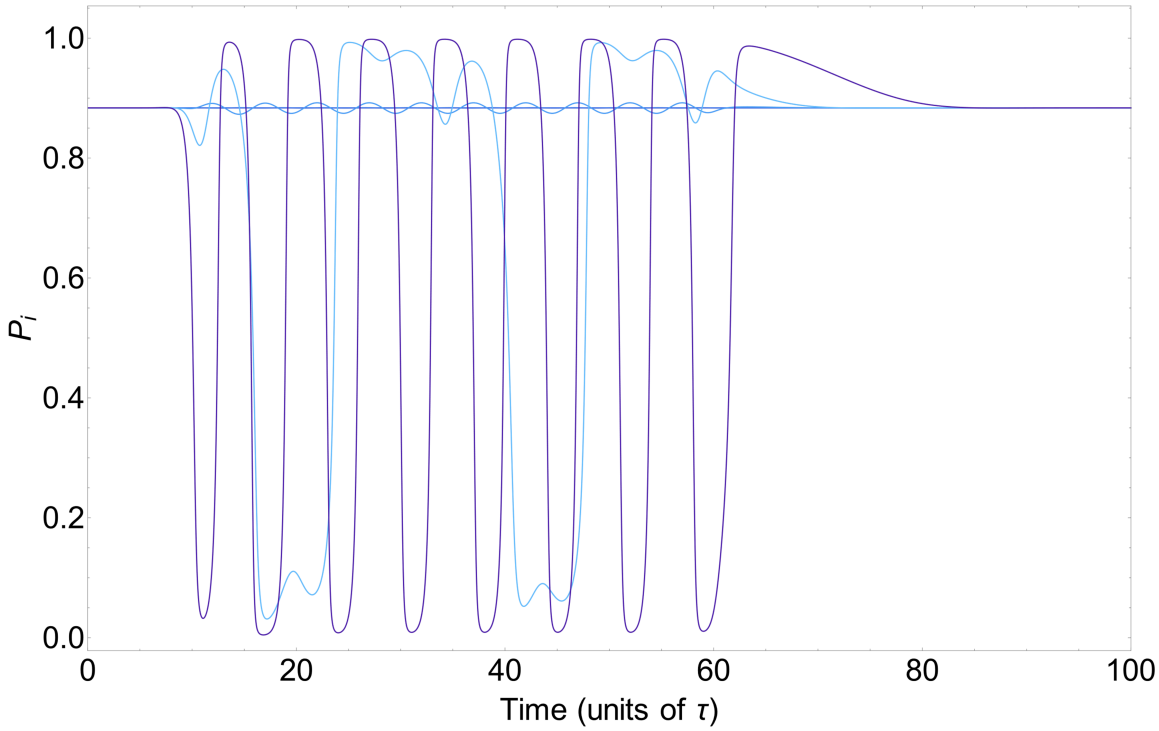

Figure 2.3: **Healthy reaction.** A plot of P_i for an array of healthy hair cells reacting to a finite duration sinusoidal signal.

2.3.2 Tinnitus Behavior

With larger coupling strength, the hair cell array can exhibit sustained activity even in the absence of external stimulation. An example is shown in Figure.2.4. We identify this sustained activity with tinnitus. In fact, for sufficiently large β sustained activity is observed even without an initial triggering stimulus.

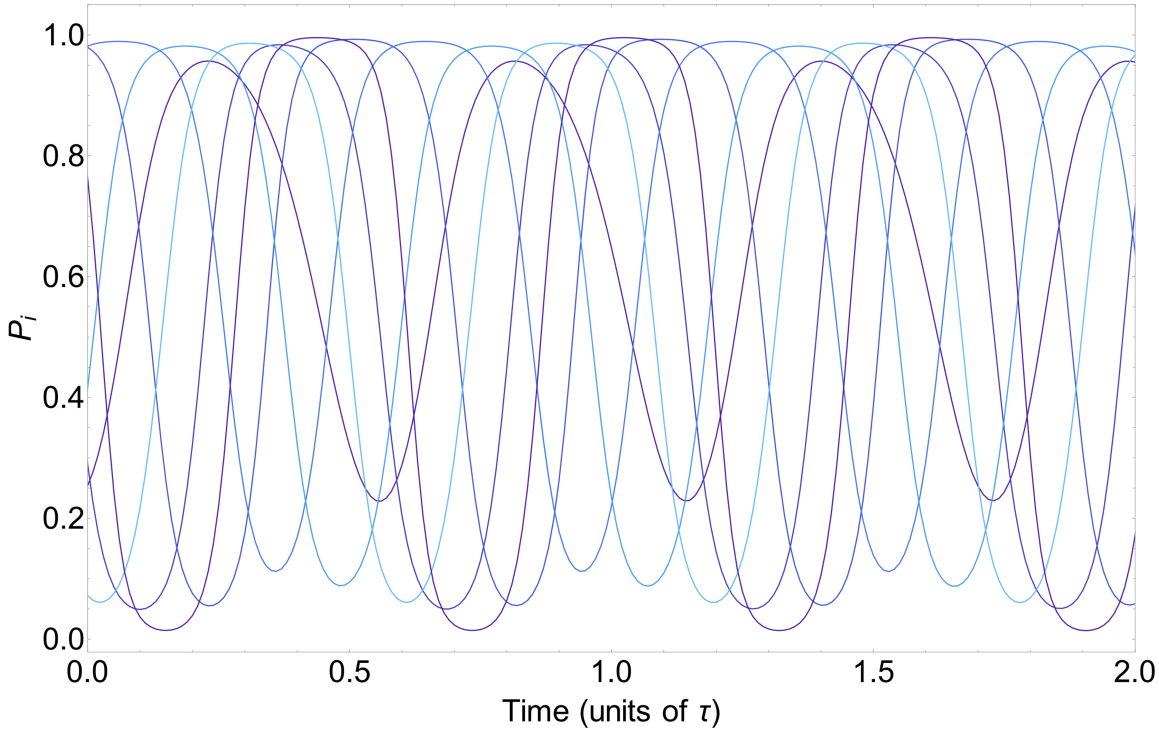

Figure 2.4: **Tinnitus behavior.** A plot of the P_i for members of an array of hair cells that are strongly coupled. The cells remain active even after the external signal ends.

Extensive simulations lead to a fuller picture of the fundamental underlying dynamics, as is summarized in Figure 2.5, representing the β-S parameter plane. For low coupling between the elements (small β), there is a single stationary point. This point can be either stable or unstable depending on the value of the single-element parameter S, in keeping with the results of Ref. [23]. S is proportional to the concentration of ions in the fluid surrounding the cells and so it is not tied directly to any physical structure of the ear and is the most plausible parameter to vary significantly. As β is increased, the system exhibits a new attractor corresponding to sustained activity. Thus, the parameter plane is split into 3 regions. In the bottom left region, the only attractor is the stationary point, so all activity stops in the absence of external forcing. In the middle region the stationary point and the sustained-activity attractor are both stable: depending on the details of the forcing stimulus, tinnitus is possible,

but not inevitable. In the third region, only the active state is attracting. While sustained oscillatory behavior is not necessarily indicative of an unhealthy state, the oscillations of the P_i quickly become much higher energy and frequency than those of the Nadrowski system as coupling increases, oscillating on the order of audible frequencies.

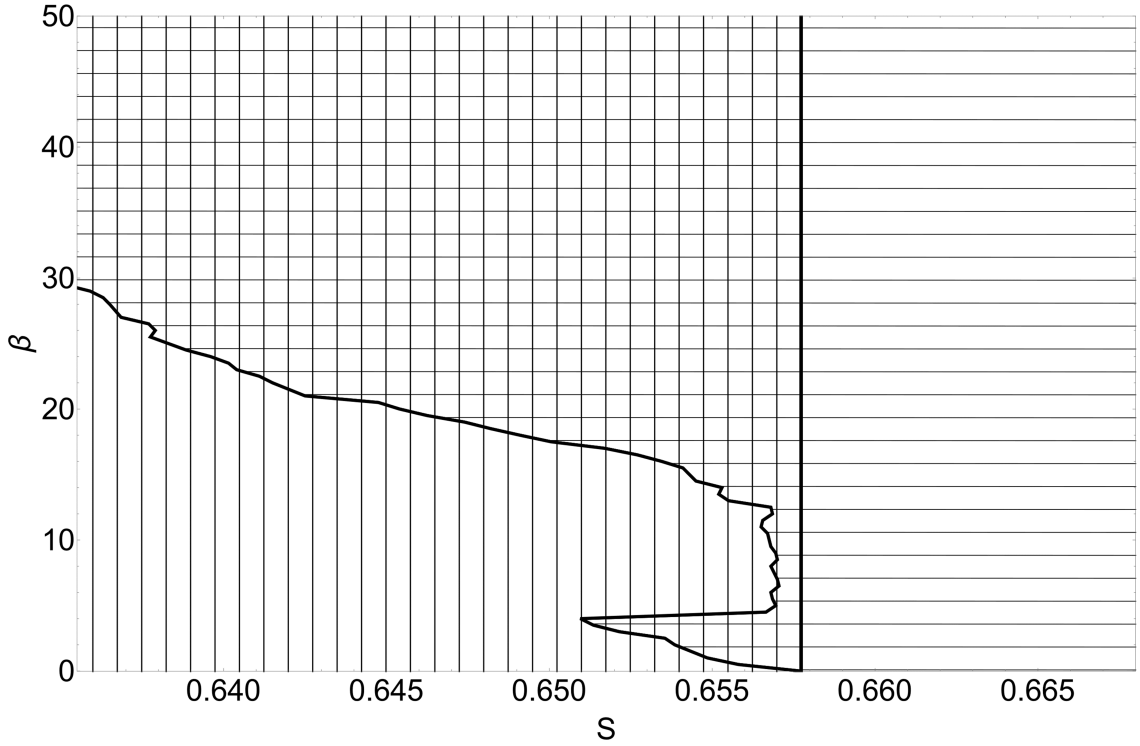

Figure 2.5: **Parameter space.** $\boldsymbol{\beta}$ and $\boldsymbol{S}$ parameter space showing long term behavior of the system. The region with vertical hatching is where the stationary point is stable, and the region with horizontal hatching is where the active attractor is stable.

2.3.3 Response to Therapy

The goal of therapy is to affect long term change of the system. To account for gradual changes, we modified our model by allowing the nominally constant coupling parameter to adjust on a very long time scale, as we now describe. The essential physical idea is that unceasing hair cell activity inhibits the natural relaxation of β back towards lower values. To make this idea quantitative, we divide the array into groups of three indexed by k. The local activity α_i is defined as the amplitude of the

sum of the P_i over the local neighborhood denoted by Ξ_k (Equation.2.8). Ξ_k consists of the elements in group k and in adjacent groups. The schematic Figure.2.6 illustrates the situation. This formulation gives a larger number for α if the oscillations of P for nearby cells are large and synchronized. If either the activity of the cells is low or desynchronized with the nearby cells, then α_i is small. All the α_i in a group are equal. The dynamics of β_i given in Equation 2.9 allows β_i to increase with large α_i and decrease with small α_i. S is then a function of the average over the entire system of the β_i in a similar way. This feedback between the instantaneous state of the system and its slower varying parameter values is what allows for dynamical healing of the system. For example, if the members of a group move together, the coupling between them and their neighbors will increase, intensifying the excitation of their neighborhood and causing a feedback that keeps that activity going. Eventually the parameters can drift into the unhealthy region of Figure 2.5 where activity can persist indefinitely.

Thus, we add to Equations.(2.4 - 2.6) the equations for the (slow) evolution of parameters β_i and S:

$$\alpha_i = \eta \mathrm{Amp}\left(\sum_{\Xi_k} P_i\right) \tag{2.8}$$

$$\Lambda_\beta \beta_i{}' = \alpha_i - \frac{\beta_i}{1+\alpha_i^2} \tag{2.9}$$

$$\Lambda_S S' = \bar{\beta} + \frac{-\nu}{1+\left(\frac{1}{10}\bar{\beta}\right)^2}\left(S - \frac{1}{2}\right) \tag{2.10}$$

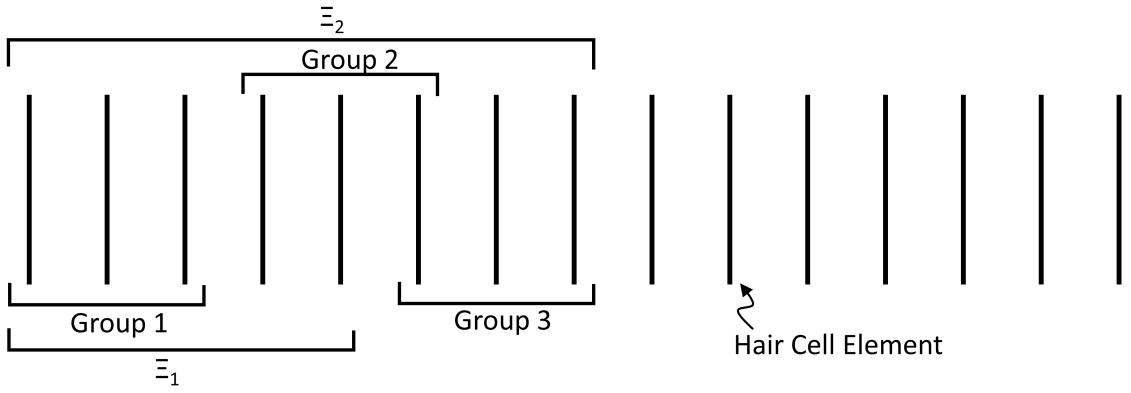

Figure 2.6: **Groupings of cells.** Schematic showing the grouping of elements used to calculate the α_i.

where η is a constant that controls the scale of the activity in the system; and Λ_β and Λ_S are constants setting the time scale of the evolution of the parameters β and S, respectively. In the simulations reported here, $\eta = 25$, $\Lambda_\beta = 1 * 10^3$, $\Lambda_S = 1 * 10^{10}$, so that β evolves with a characteristic time on the order of minutes; slower than the oscillations of the hair bundles, but faster than the long term healing process. Meanwhile, S evolves with a characteristic time on the order of weeks. $\nu = 2 \times 10^3$ and characterizes the strength of negative feedback on the value of S. In simulation, the amplitude of the signal was calculated in a short moving window of time behind the current integration time.

In the clinical trials [1], subjects listened to a series of pure tones. The tones were selected to be close to the frequency of the subject's tinnitus, and such that the stimuli excited hair cells that were equally spaced along the basilar membrane. The tones were turned on and off at a frequency much lower than the frequency of the tones. Each therapeutic session lasted a few hours, with sessions repeated daily, for a period of weeks. To apply therapy to our system an F_i was added.

$$F_i(\tau) = T_i(\tau)G_i, i = 1...N \tag{2.11}$$

$$T_i(\tau) = k\left(\sin\left(\frac{2\pi\tau}{i}\right) + \omega\right) \tag{2.12}$$

$$G_i = \sum_j e^{-(i-j)^2}, j = 2, 5, ...N-1 \tag{2.13}$$

In our simulations, $k = \omega = 15$.

Each element reacts to a specific tone whose frequency is a monotonically decreasing function of its spatial location. This is due to the structure of the cochlea which causes different hair cells to respond to different frequencies depending on their location along the basilar membrane. This spatial dependence is included in the $T_i(t)$ term of Equation 2.11. It is a sinusoidal function that is also turned on an off at a frequency faster than the transient time of the system, but slower than the frequency of vibration of any affected element. For a typical system, in units of dimensionless time, the transient time is on the order of $\sim$100 and the period of oscillations of a driven elements is on the order of $\sim$1 so the driving signal is turned on and off with a period of 50. This allows the therapy to desynchronize the elements by driving them at their different natural frequencies, while also taking maximum advantage of transient disorder. The G_i term controls how strongly the elements respond to the stimulus as a function of their spatial location—in this case a series of equally spaced smooth Gaussian envelopes. This matches the spatial distribution of external forcing in the coordinated reset theory used in the clinical trial as a series of tones equally spaced along the basilar membrane [1, 27].

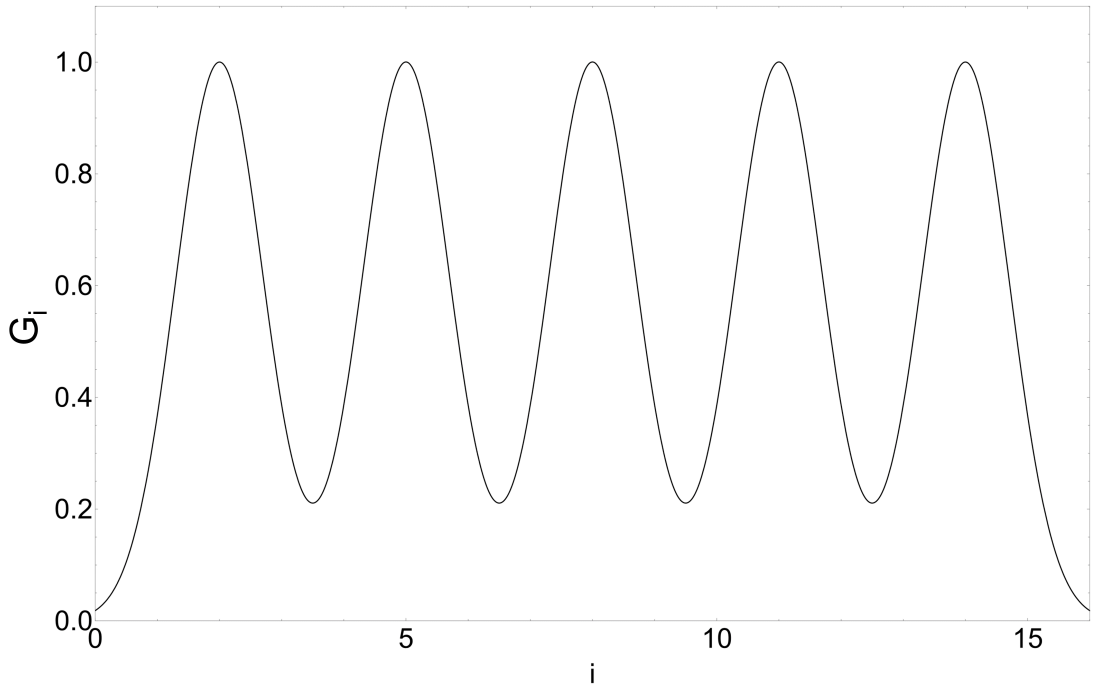

Figure 2.7: **Spatial part of external intervention signal.** G_i from Eq. 2.11. Equally spaced Gaussian groups of effected elements as a function of spatial index i.

Figure 2.8 shows a typical progression of the system starting from an active (unhealthy) state. The above therapy is then applied. This slow evolution of S can allow the system to remain in an unhealthy(active) state after multiple rounds of therapy. In this case, it would require more repeated applications of the therapy in order to move the system into a healthy region of parameter space. When the therapy is discontinued and the system is still in a state of tinnitus, it eventually returns to its initial state of behavior.

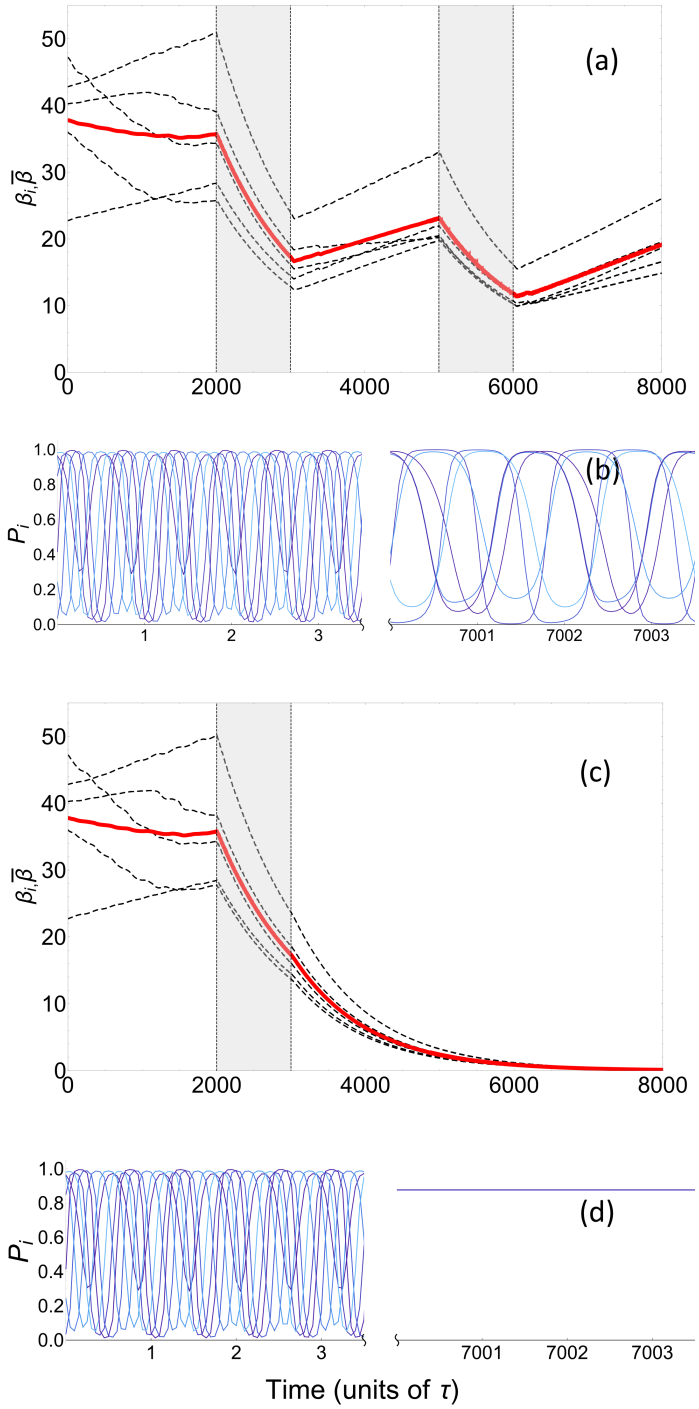

Figure 2.8: **Effect of system intervention.** The shaded regions are times when a therapeutic signal was applied. The red lines are averages of the β_i. The evolution of S is slow enough to allow the persistence of tinnitus symptoms if the system has not moved into the stable parameter region. The only difference between plots (a) and (b) and plots (c) and (d) is the initial value for S. (a) The behavior of the β over a series of therapy applications with an initial S value of .65. (c) The behavior of the β over a series of therapy applications with an initial S value of .64. (b) The detailed behavior of the P_i before and after two periods of F_i corresponding to the intervention in (a). (d) The detailed behavior of the P_i before and after a single period of F_i corresponding to the intervention in (c).

2.3.4 Discussion

Our model assumes that the underlying cause of the pathology can be treated indirectly by treating the symptoms of the etiology. This is not something that is initially obvious, but the clinical data is encouraging of this form. A dynamical, noninvasive approach to therapy supposes a gradual drift of system parameters into an unhealthy region of parameter space, with the possibility of forcing the system back to a healthy region. The sudden onset of symptoms does not exclude this approach; however it is most likely not applicable to cases of tinnitus caused by injury or physical damage to the system. Rather, the dynamical picture explored in this chapter is useful in understanding tinnitus without a clear external cause as a relaxation of parameter values or a feedback in the system reinforcing unhealthy behavior. Tinnitus is a symptom that can have a multitude of causes involving action and interaction of the inner and outer ear, neurological, cardiovascular, and skeletal systems. Ours is a simple model for only part of the inner ear. Nevertheless, the reproduction of key features of clinical data suggests that this model can be a constructive tool in the investigation of tinnitus.

The fact that very similar desynchronization schemes works well in the context of mechanical hair cells as well as neurological models [27] shows a robustness of coordinated reset therapy with respect to the specific details of the systems. A similar therapy could be used to treat other disorders thought to be caused by over-synchronization of neurons. For example, delayed feedback deep brain stimulation has been proposed for treatment of Parkinson's disease, essential tremor, and other neurological disorders where over-kindling is thought to play a role [33]. The robustness of the desynchronization scheme above supports an open-loop deep brain stimulation that would not require continuous monitoring of brain activity.

2.3.5 Criticality

The parameter values used in simulation can be found in Table 1 of [23] except for f_{max} which takes the value of $370pN$. This parameter was changed from $352pN$ in order to place the system initially in the unhealthy parameter space. Many of the parameters have been experimentally determined. These natural parameter values place the system close to an oscillatory instability [23]. f_{max} was altered to place the system inside the oscillatory region of parameter space. There is experimental [32, 34] and theoretical [23, 32, 35] evidence that the ability to hear very quiet sounds and distinguish similar frequencies arises from proximity to this type of criticality.

This is just one example of many of a biological system that seems to be poised near a critical point [36]. The natural fine tuning of the parameters of the cochlear system appears to maximize audio sensitivity, but could also help explain the onset of conditions like tinnitus, by allowing relatively small drifts in system parameters to cause significant qualitative changes in the behavior of the system. Fortunately, this can also allow a path back into a healthy state of the system without drastic or invasive intervention. If a slow wandering of parameters causes pathology, it could also restore healthy behavior. In a living system, homeostatic mechanisms can be what hold the system near a critical point. There are numerous hearing disorders that are the direct result of disrupted ion homeostasis. As suggested by Trune:"While the initial cause may be something else (inflammation, ototoxicity, noise, etc.), the ultimate impact on the ear is the interference of some ion or water transport mechanism. Thus, impaired ion homeostasis is essentially the final common pathway for many inner ear diseases" [37]. Because the cochlear system operates near an oscillatory critical point, disrupting these mechanisms can cause qualitative dysfunction including spontaneous activity.

2.4 Abstract Model

The above model is based on a different part of the human auditory system (the cochlear rather than the auditory cortex) than the one coordinated reset therapy was designed for and this difference comes out in the details of the proposed therapy, but the general behavior is similar in both models. For example, the original coordinated reset theory was based on a model of neuronal oscillators with normally distributed natural frequencies. This means that the different elements had to be forced at different times to "unkindle" them with their neighbors [1, 31]. The different natural frequencies of the hair cell elements eliminate the need for this time delay, so they can all be forced at one time. Both models show states of rest or passive activity based in part on the strength of the coupling between their elements. Both systems respond to a similar desynchronizing external signal with short term desynchronization. Also, there is evidence for both systems operating near a criticality [34, 35, 38]. Here we explore what is essential for a system to exhibit tinnitus-like behavior through a more abstract model of simple coupled oscillators without any detailed physiological dynamics.

We develop a system with a few key characteristics. First, it is an array of oscillators that have a sense of phase and amplitude. Next, activity in nearby elements can excite or maintain activity in other members. Lastly, the coupling strength between elements is a function of the overall activity of the system. These elements allow for the system to have different behaviors depending on coupling strength. A quiescent state that returns to zero activity in the absence of external driving, and an active state that maintains activity on its own. We begin with the equations for

the oscillators and their coupling strength.

$$\lambda_r \dot{r}_i = r_i \left(k R_i S_i - \lambda + F_i(t) \right) \qquad , i = 1...N \tag{2.14}$$

$$\lambda_k \dot{k} = K_1 K_2 \tag{2.15}$$

The system is an array of oscillators with amplitudes r_i, and nearest neighbor coupling strength k. $K_1 = k(k_{\max} - k)$ and constrains k to be positive and saturate at $k = k_{\max}$. K_2 is a function of the average amplitude of the oscillators, $\alpha = \frac{1}{N} \sum_i^N r_i$, and controls how the coupling strength evolves as a function of of the r_i. k will increase if the average of the amplitude of the oscillators is above the threshold a and decrease otherwise.

$$K_2 = \frac{1}{1 + \exp(a - \alpha)} - \frac{1}{2} \tag{2.16}$$

With the parameter values chosen here the coupling will typically be driven up if there is more than one active group and be driven down otherwise. R_i is a function of the r_i and assures that an oscillator can only feel an effect from its neighbors if it is active, meaning it has an amplitude above threshold b.

$$R_i = \frac{1}{1 + \exp(b - r_i)} \tag{2.17}$$

S_i is the coupling term and allows the neighbors of an active oscillator to drive its amplitude higher if they are in phase with one another with a phase $\theta_i = \pi r_i$.

$$S_i = C(r_{i-1}) \cos(\pi(r_i - r_{i-1})) + C(r_{i+1}) \cos(\pi(r_i - r_{i+1})) \tag{2.18}$$

The multiplicative term $C(x) = \left(\frac{x^2}{1+x^2} \right)$ makes sure that a neighboring oscillator only has an effect if it has an amplitude larger than 0. λ is a positive constant that

drives the amplitude of an oscillator down in the absence of internal synchrony or external driving $F_i(t)$. Plots of these terms are shown in Figure 2.9. This means that each oscillator has an amplitude and a phase and the degree of synchronization between two members can naturally be the difference in phase between them. In the simulations shown here, $N = 20$ and the parameter values are $\lambda_r = 10$, $\lambda_k = 1000$, $k_{\max} = 15$, $a = 7.5$, $b = 30$.

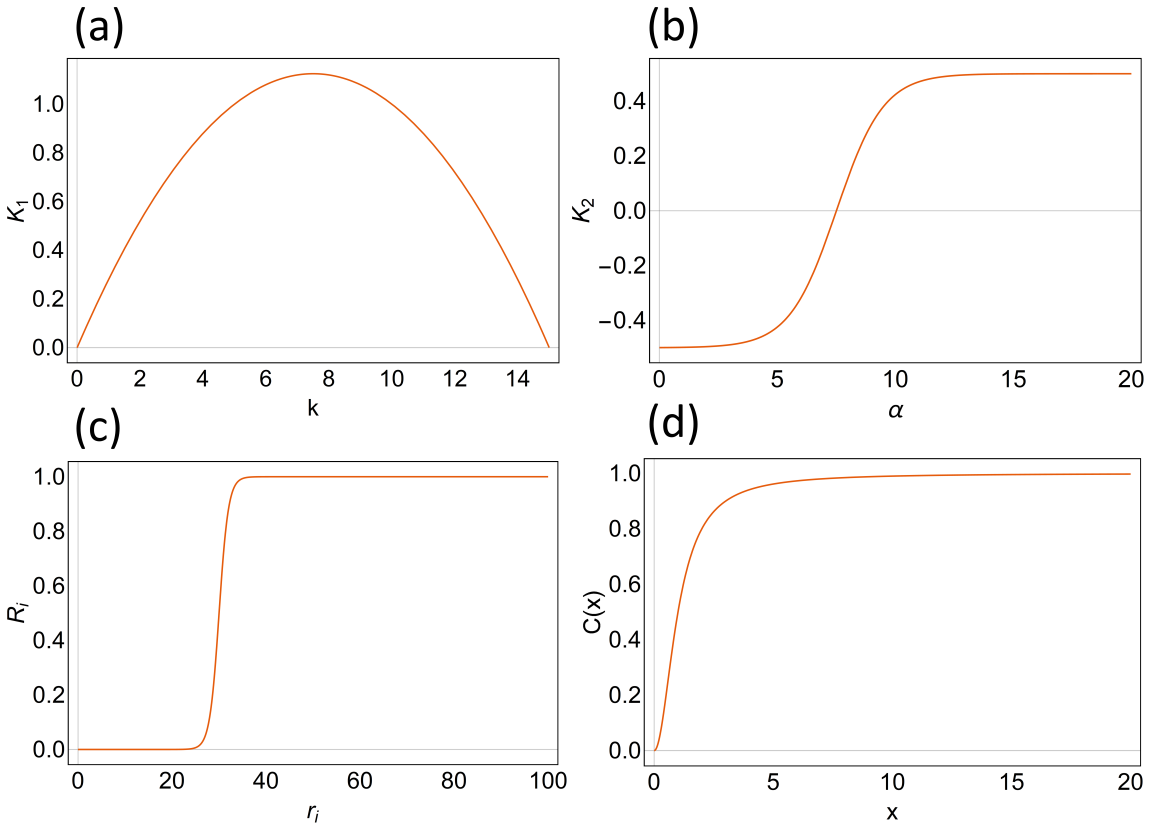

Figure 2.9: **Dynamical equations terms.** (a) K_1 is a parabola that constrains the coupling of the system to be positive and saturate at k_{max}. (b) K_2 is a function that controls how the coupling strength varies as a function of the activity in the system. It is negative when activity is low and positive when activity is high. (c) The function that controls where the threshold is between the amplitude of an active and inactive oscillator. Here the threshold is $a = 30$. (d) $C(x)$ is a function the assures that neighboring oscillators only affect each other is they have non zero amplitude. x is a dummy variable that is replaced with the applicable r_{i+1} or r_{i-1}.

2.5 Behavior

There are two possible overall behaviors of the system depending on coupling strength. If the coupling strength $k < \frac{\lambda}{2}$ then the $\dot{r}_i$ is always negative because $kR_iS_i < \lambda$ and the mutual interaction between neighbors is too weak to sustain activity. In this situation the system settles at the universally stable stationary point at $r_i = 0$. If $k > \frac{\lambda}{2}$ then there is still a stationary point at $r_i = 0$ and the same behavior as before is common, but and there is also an infinite number of configurations where $kR_iS_i \geq \lambda$ and some neighboring members are close enough in phase to maintain their amplitude. The larger k, the more separated the phases of a group of oscillators can be and still not decay to zero. This behavior can be seen in the example trajectory shown in Figures 2.10 and 2.11.

In a typical evolution of the system from a random initial condition with $k > \frac{\lambda}{2}$ in the absence of external driving the majority of the amplitudes go to zero. A few small groups of oscillators maintain a higher amplitude because they are active and have a close enough phase with their neighbor. This behavior is show in Figure 2.10. In this case there are two surviving groups of activity, each with two members. This level of activity is enough to push the coupling strength k up to 15.

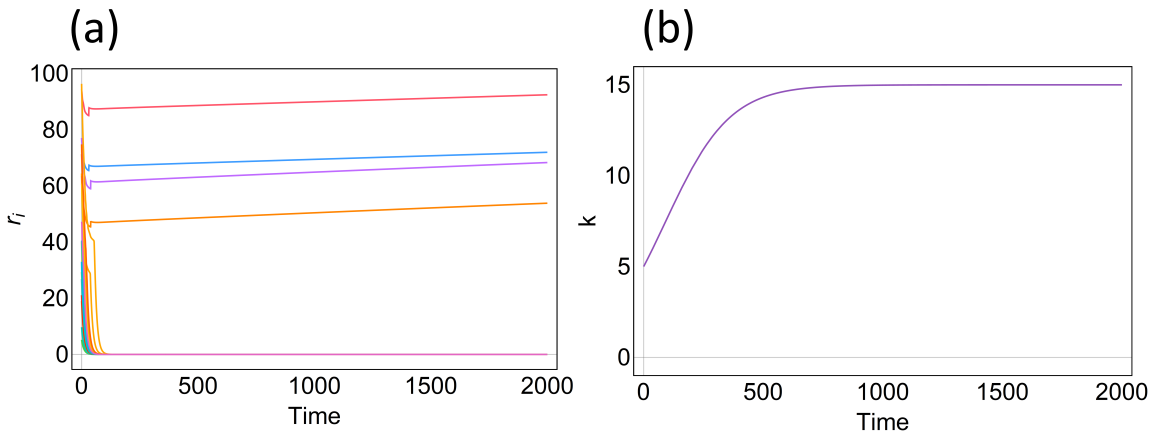

Figure 2.10: **Behavior of abstract system.** The system of oscillators with random initial conditions. Two groups of two oscillators maintain their amplitude through mutual interaction. The average amplitude of the members is enough to increase the coupling. (a) is a plot of the r_i. (b) is a plot coupling constant k.

Figure 2.11 shows the final configuration of the trajectory from Figure 2.10 in r–θ space. The solid black curve represents the $\theta = \pi r$ spiral that each oscillator is confined to move on. The red dot at the origin is the collection of oscillators that have decayed to zero amplitude. In green and blue are each of the pairs of neighboring oscillators that have maintained their activity. The differences in phase within each group mod 2π is about $\cos^{-1}\left(\frac{1}{k}\right)$.

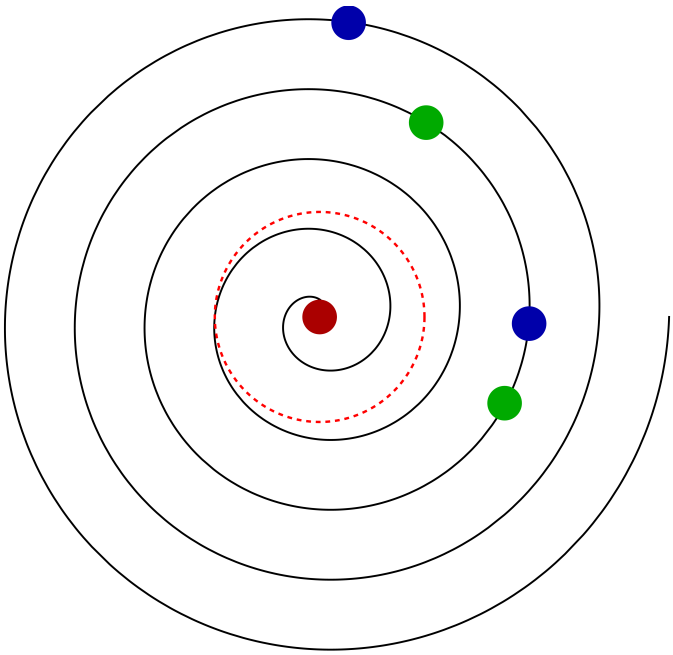

Figure 2.11: **Final state example.** Colored in red are the oscillators that have settled to zero amplitude. Green and blue are each groups of oscillators that have synchronized enough to maintain their amplitudes. The solid black curve represents the spiral that the oscillators are confined to move on (for illustrative purposes the spiral is displayed here is not as tight as the exact one). The dashed circle has a radius of a and represents the threshold of amplitude where an oscillator is considered active.

In a run of this system from random initial conditions the oscillators ride the spiral towards the center, being pushed inward by λ. They continue to spiral inward unless two physically adjacent oscillators fall within $\sim \cos^{-1}\left(\frac{1}{k}\right)$ of each other in θ before either amplitude becomes less than a(inside the red dashed circle in Figure. 2.11). In that case they can maintain each other's amplitude as long as the coupling strength remains high enough.

2.5.1 Intervention

When the system finds a configuration that perpetuates activity it requires external intervention to get kicked out of that stationary point. Here we use an external

signal similar to the previous section.

$$F_i(t) = u \exp\left[-\left(\frac{i-\mu}{\sigma}\right)^2\right] \sin(t) \tag{2.19}$$

The temporal part of this signal is a simple sinusoid that drives the affected oscillators back and forth. The spatial part is a Gaussian that confines the drive to the local area of an active group. Here we center the signal on one of its members. Shown in Figure 2.12 is the effect of this intervention on the same system from Figure 2.10. The signal knocks one of the groups out of its stationary configuration and the oscillators become separated enough in phase to decay to zero amplitude. After the external signal is removed the average activity of the oscillators is not enough to drive up the coupling strength anymore and the coupling strength drops until $k < \frac{\lambda}{2}$ and the origin becomes a global attractor.

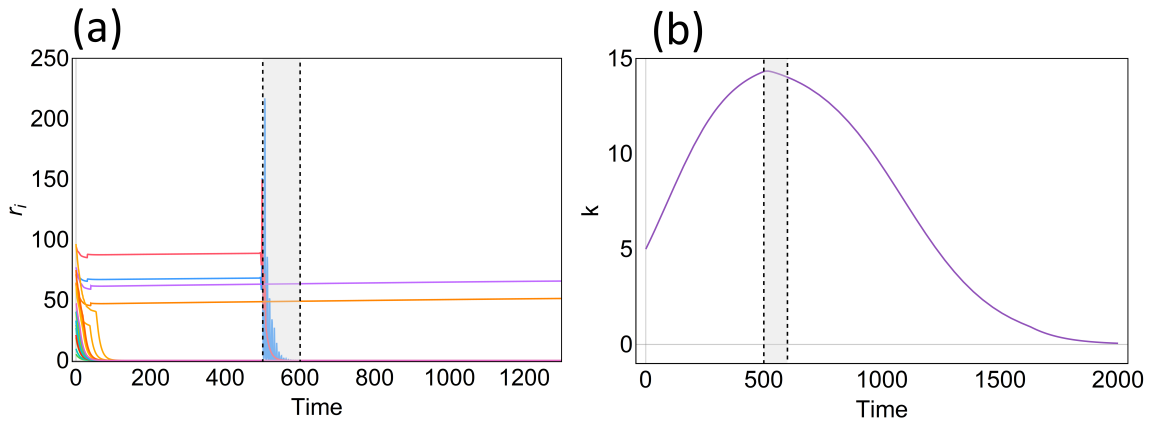

Figure 2.12: **Behavior with intervention.** The system of oscillators with external intervention. The shaded region is where the intervention signal is applied. The external signal desynchronizes one of the groups, allowing the coupling to fall. Eventually the coupling is too weak and all activity stops.

2.5.2 Discussion

The above oscillator model demonstrates a few key attributes that should be found in any dynamical theory for tinnitus. First, the system has a "healthy" regime that

will react to an external signal but will cease activity when that external signal is removed. Second is a "tinnitus" regime where even when there is no external signal applied the system, activity is self-sustained. Third is an ability of the system to dynamically move between these two regimes. This is accomplished by varying some parameters in the system as a function of the motion of the oscillators. The feedback between the state of the system and the structure of its attractors can help explain the onset of an ailment like tinnitus through an incremental degradation process rather than any sort of sudden irreversible damage and also allows the system to be driven into the healthy regime from the unhealthy one by driving the dynamics directly. If the natural state of the system is near a critical point, then a relatively small incremental change in parameter values can drastically change the behavior of the system. Specific to the case of tinnitus, it appears that desynchronization of neuronal or hair cell oscillators can put the body in a position of natural healing. In this case the therapies employed have been designed to take advantage of the fact that different oscillators in the same array feel a different driving even if there is one external signal being applied to the physical system as a whole. For instance, in the case of the organ of Corti, the shape of the organ as well as the interaction between membranes of tissue and a column of fluid create a situation where mechanical waves of different frequency effect different parts of the basilar membrane more strongly. This means that specific members of the oscillator population can be targeted. This is key to the coordinated reset desynchronization scheme because, of course, if two similar elements are synchronized and they are driven by the same signal, they will remain synchronized.

One recent study that could be understood in a similar dynamical disease context was done on mice by Garza et al. [39]. Mice were put in a cage with LED lights on one side and exposed to different frequencies of flashes for different lengths of time. It was found that this exposure increased the 40Hz (gamma) neural activity in the mice's

brains which in turn increased activation of part of the neuroimmune system and decreased the production of a protein (amyloid-β) that accumulates in Alzheimer's disease. Exact mechanisms for why the driving of neuronal activity in the gamma range cause an immune response are unknown. The dynamical disease story goes as follows: The patient has a disease that is causing the excessive buildup of this protein. The patient's natural immune response would have the ability to reduce, slow, or halt this buildup but is suppressed because of their current unhealthy state. By driving the gamma range of frequencies in the patient's brain through visual stimulation and synchronizing their neural activity, the patients physiology is now in a state that facilitates their immune response and the ailing buildup is reduced. This kind of therapy is desirable if the direct treatment of the protein accumulation is difficult or impossible.

2.6 Summary

In this preceding chapter we introduced a dynamical model to explore both the onset of tinnitus and the effects of coordinated reset therapy. This model extends an existing theory of individual outer hair cell dynamics to include their mutual interaction and considers how sustained activity can inhibit the natural recovery process. The model shows behavior broadly similar to that reported in the clinical study. We then develop a similar, more abstract model that exhibits the essential components of a dynamical theory for tinnitus-like behavior.

Chapter 3
Kinetic Theory of Directed Supersmarticle Motion

3.1 Introduction

Robots are usually built as a cohesive whole in order to achieve a specific task. This is unlike biological multicellular organisms which are made up of a large number of much smaller strongly interacting agents. The collective action among a population allows for flexibility of action for different purposes and in different environments and also gives room for fault tolerance [40]. One of the most basic of these actions is locomotion. In this chapter we describe and model the diffusive motion of a collection of interacting, but non-communicating, simple robots. A small, battery powered, three link robot that can deform itself through movement of its arms known as a "smarticle" was developed in the Goldman lab (Shown in Figure 3.1a). When a smarticle is placed on its side it cannot translate or rotate on its own because its arms do not come in contact with the surface it is sitting on. Movement can only take place through interaction with other objects, such as other smarticles [2].

The dynamics focused on here will be of the "supersmarticle". A supersmarticle is a collection of smarticles enclosed in an unanchored ring, Figure 3.1b. When the smarticles deform, they push on each other and the ring. Translation of the ring is then possible. Experiments show that when all internal smarticles are performing a periodic gate, the ring can translate, but does not have a preferred direction. It was found that when one smarticle is made inactive and in a straight configuration the supersmarticle drifts on average either towards or away from the inactive smarticle,

depending on the mass of the enclosing ring. To better understand this biased motion, we develop a collision model for the system.

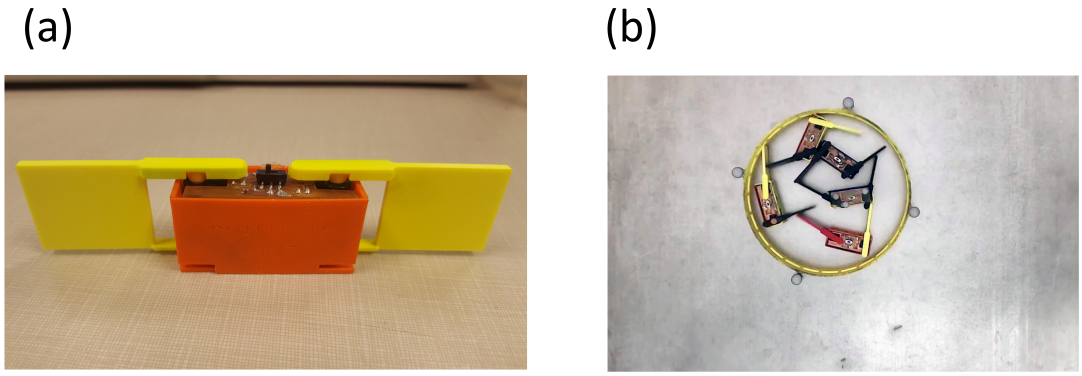

Figure 3.1: **Smarticle and supersmarticle.** (a) A smarticle in the "straight" position. (b) A supersmarticle with 5 smarticles

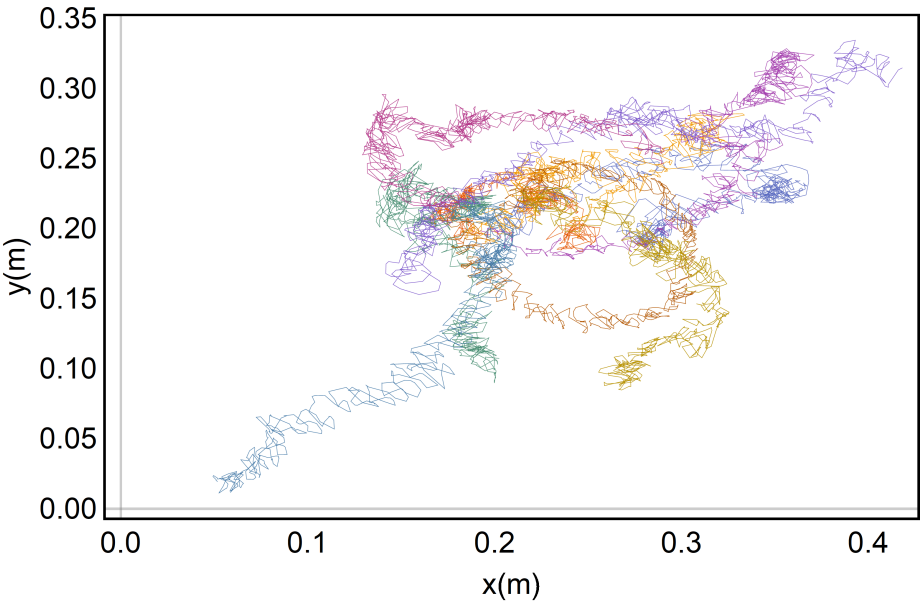

Figure 3.2: **Sample Trajectories.** Shown are a collection of smarticle trajectories. The systematic drift of some of the trajectories is evident, as well as the jagged motion that suggests a series of sudden nudges rather than a smooth continuous motion.

3.2 Supersmarticle Theory

We represent the active matter system with a stochastic two-dimensional scattering model consisting of a ring, a group of active smarticles, and an inactive robot in a straight, fixed position. The active robots act on the ring with a series of small nudges. In principle, the motion of the ring is a function of the exact state $\mathbf{\Omega}(t)$ of the smarticle/ring system just before each collision. This state includes all of the relative positions and momenta of the smarticles and the ring. It is enough information to say exactly how every component of the system will be affected by each collision. Each collision causes a displacement of the ring $\mathbf{\Delta R}(\mathbf{\Omega}(\mathbf{t}))$. If the system is in state $\mathbf{\Omega}$ with probability $P(\mathbf{\Omega})$ then the mean displacement of the ring can be written $\langle \mathbf{\Delta R} \rangle = \int P(\mathbf{\Omega}) \mathbf{\Delta R}(\mathbf{\Omega}) \, \mathrm{d}\mathbf{\Omega}$. The complicated interactions between the smarticles and the ring as well as between the smarticles and each other mean that both $\mathbf{\Omega}$ and $P(\mathbf{\Omega})$ are highly sensitive to initial conditions and difficult to measure and so we develop a simplified model.

3.2.1 Collision Types

A collection of trajectories of supersmarticles with all the same ring mass are shown in Figure 3.2. One thing that is obvious about these trajectories is that the motions of the supersmarticles can vary widely from trial to trial even if there is an average drift among many trials. Another thing that is obvious is that the trajectories are jagged even though the time resolution of the data is high (about a tenth of a second). This leads us to a probabilistic collision model to allow for the variability in possible behavior and the apparent discrete nature of movement events.

$\mathbf{\Omega}$ is reduced to the direction of the nudge, and whether or not the inactive smarticle is in contact with the ring. This leads to a statistical model with two random variables. The first is an angle Θ which represents the direction of an individual

nudge and takes a value between 0 and 2π. The second is a binary variable β which represents whether the inactive smarticle is in contact with the ring or not. A cartoon and schematic of the system is shown in Figure 3.3. Depending on the value of these two random variables, an individual nudge can either move just the ring, just the inactive smarticle, or both the ring and the inactive smarticle. We assume that $P(\mathbf{\Omega})$ is isotropic so each nudge has a uniform probability to act in any direction.

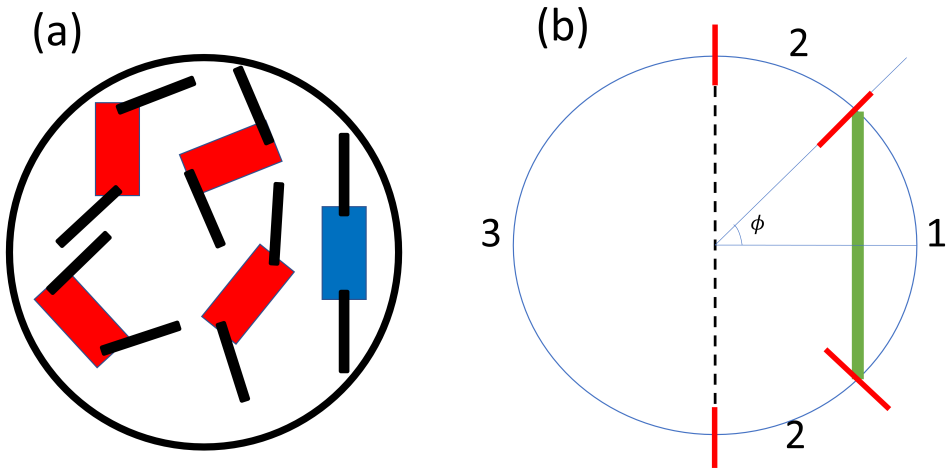

Figure 3.3: **Supersmarticle system schematic.**(a) A cartoon of the supersmarticle system, with 4 active smarticles in red and one inactive smarticle locked in the straight position in blue. (b) A schematic of ring, with the green bar representing the inactive smarticle. Numbers identify sections of the ring that correspond with Table. 3.1. ϕ is the angle that characterizes the size of the inactive smarticle.

There are six different types of collisions depending on whether the inactive smarticle is in contact with the ring, and which region of the ring the nudge acts on. Each of these collision types will either move both the ring and the inactive smarticle, just the ring, or cause no ring movement. These possibilities are summarized in Table 3.1.

Table 3.1: A tabulation of what is moved and in what direction for the different types of collisions as a function of Θ and β. $\beta = 1$ when the inactive smarticle is in contact with the ring and $\beta = 0$ when the inactive smarticle is not in contact with the ring.

Region	$\beta = 1$	$\beta = 0$
1	Both towards inactive	No Movement
2	Ring towards inactive	Ring towards inactive
3	Both away from inactive	Ring away from inactive

3.2.2 Mean and Variance of Average Velocity

We call the distance that a nudge will displace the ring R_A when moving only the ring and R_B when moving both the ring and the inactive smarticle together. Denoting the fraction of time that the inactive smarticle is in contact with the ring as λ, the frequency of nudges as f, the amount of time the supersmarticle has been active as T, and each nudge as $\mathbf{x}_i$, the mean of the velocity of the supersmarticle in the direction towards the inactive smarticle is

$$\begin{aligned}
\langle v_\parallel \rangle =& \left\langle \frac{\sum_i^N x_{i\parallel}}{T} \right\rangle = \frac{N}{T}\langle x_\parallel \rangle = \frac{fT}{T}\langle x_\parallel \rangle = f\langle x_\parallel \rangle \\
=& f\left[\frac{1}{2\pi}\left(\int_{-\phi}^{\phi} \lambda R_B \cos(\theta) d\theta + 2\int_{\phi}^{\pi/2} \lambda R_A \cos(\theta) d\theta + \int_{\pi/2}^{3\pi/2} \lambda R_B \cos(\theta) d\theta \right) \right. \\
& \left. + \frac{1}{2\pi}\left(2\int_{\phi}^{\pi/2} (1-\lambda) R_A \cos(\theta) d\theta + \int_{\pi/2}^{3\pi/2} (1-\lambda) R_A \cos(\theta) d\theta \right) \right] \\
=& \frac{f}{\pi}[\lambda(R_A - R_B)(1 - \sin(\phi)) - (1-\lambda)R_A \sin(\phi)]
\end{aligned} \tag{3.1}$$

where each integral is over the appropriate angles for a specific collision type and a $\parallel$ subscript denotes motion in the direction towards the inactive smarticle. We describe the term highlighted in blue here and all other terms are obtained similarly. The integral goes from $-\phi$ to ϕ because we are integrating over ring section 1 (Figure.3.3). Inside the integral, we multiply by λ because this term corresponds to a collision type

with the inactive smarticle in contact with the ring. We multiply by R_B because this collision type moves both the ring and the inactive smarticle together. We use $\cos(\theta)$ because we are interested in the component of the motion parallel to the inactive smarticle. All of the other terms are obtained similarly for each collision type choosing the bounds for the integral from the section of the ring, choosing $\lambda(1-\lambda)$ if the inactive smarticle is in contact(not in contact) with the ring, and choosing $R_A(R_B)$ if the nudge type moves just the ring(both the ring and the inactive smarticle). The $\frac{1}{2\pi}$ is because we are averaging over θ. Notice that depending on the relative size of R_A and R_B the sign of this expression can change. R_B is always less than R_A, but in the case where $R_B \ll R_A$, $\langle v_\parallel \rangle = R_A(\lambda - \sin(\phi))$ which can be positive or negative and when $R_B = R_A$, $\langle v_\parallel \rangle = R_A(\lambda - 1)\sin(\phi)$ which is always negative. This can lead to a change in direction of the average velocity of the supersmarticle depending on the relative mass of the ring and smarticle because as the mass of the ring increases, the difference between nudging just the ring or both the ring and the inactive smarticle becomes less. The variance of this velocity is calculated in exactly the same way as the mean was calculated except we are averaging $(R_{A(B)}\cos(\theta) - \langle x_\parallel \rangle)^2$ rather than just $R_{A(B)}\cos(\theta)$

$$
\begin{aligned}
\mathrm{Var}[v_\parallel] =& \mathrm{Var}\left[\frac{\sum_i^N x_{i\parallel}}{T}\right] = \frac{N}{T^2}\mathrm{Var}[x_{i\parallel}] = \frac{fT}{T^2}\mathrm{Var}[x_{i\parallel}] = \frac{f}{T}\mathrm{Var}[x_{i\parallel}] \\
=& \frac{f}{T}\Bigg[\frac{1}{2\pi}\Bigg(\int_{-\phi}^{\phi}\lambda(R_B\cos(\theta) - \langle x_\parallel\rangle)^2 d\theta + 2\int_{\phi}^{\pi/2}\lambda(R_A\cos(\theta) - \langle x_\parallel\rangle)^2 d\theta \\
&+ \int_{\pi/2}^{3\pi/2}\lambda(R_B\cos(\theta) - \langle x_\parallel\rangle)^2 d\theta\Bigg) \\
&+ \frac{1}{2\pi}\Bigg(2\int_{\phi}^{\pi/2}(1-\lambda)(R_A\cos(\theta) - \langle x_\parallel\rangle)^2 d\theta \\
&+ \int_{\pi/2}^{3\pi/2}(1-\lambda)(R_A\cos(\theta) - \langle x_\parallel\rangle)^2 d\theta\Bigg)\Bigg]
\end{aligned}
$$

$$
\begin{aligned}
&= -(f/4\pi^3 T)[\pi^2 \sin(2\phi)\left(R_A^2 - R_B^2\lambda\right) \\
&\quad + R_A^2\big((-4\lambda^3 + 2\lambda^2 + 2)\phi + \pi^3\big((4\lambda^2+2)/(\pi^2) + \lambda - 2 + (2\phi)/\pi\big)\big) \\
&\quad - 4R_A R_B \lambda(2\lambda+1)(-\lambda\phi + \phi + \pi) \\
&\quad - R_B^2\lambda\left(6(\lambda-1)\lambda\phi - 6\pi\lambda + 2\pi^2\phi + \pi^3\right) \\
&\quad - 2(-\lambda\phi + \phi + \pi)(R_A - R_B\lambda)(4\lambda(R_A - R_B)\sin(\phi) \\
&\quad + \cos(2\phi)(R_A - R_B\lambda))]
\end{aligned}
\tag{3.2}
$$

As a sanity check for this calculation we perform a sampling of the probability distribution of displacement totals in the parallel direction for three different ring masses and plot them together with the normal distribution corresponding to the calculations above in Figure. 3.4.

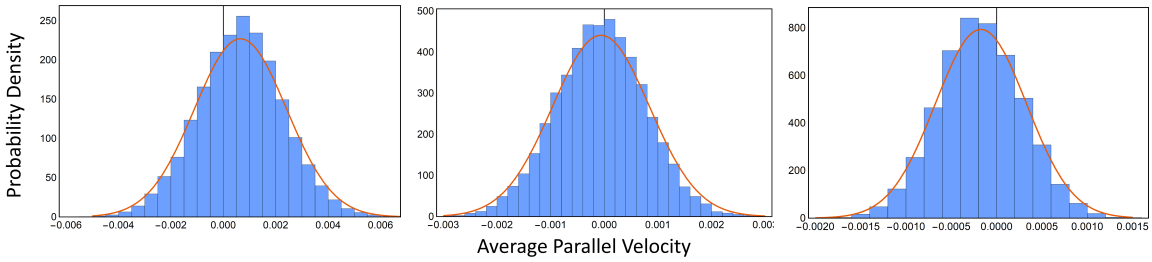

Figure 3.4: **Histograms and Distributions** A sampling of 10000 displacement totals taken from the probability distribution of collision types plotted together with the normal distribution with the corresponding mean and standard deviation from Equations 3.1 and 3.2.

To establish the relationship between the mass of the ring and distances R_A and R_B we model the active smarticles as pistons pushing on a sliding mass. A cartoon of the setup is shown in Figure 3.5. m_1 represents the arm of a smarticle, m_2 represents the body of a smarticle, and the relative distance between them is specified by the smarticle gate. The mass they are pushing on is m_b which can be the mass of the ring or the total mass of the ring and the inactive smarticle together. Both m_2 and m_b have friction between them and the surface they are sitting on.

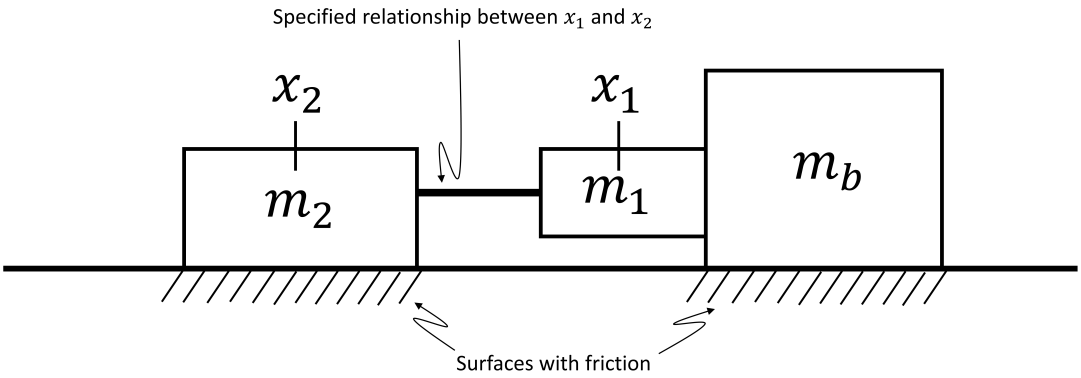

Figure 3.5: **Piston model.** A cartoon of the model for the movement of a single nudge.

This model implies the equations of motion for x_1 and x_2:

$$m_2\ddot{x}_2 = F_2 - f_s \tag{3.3}$$

$$(m_b + m_1)\ddot{x}_1 = f_s - F_b \tag{3.4}$$

Where F_2 and F_b are the friction forces on m_2 and m_b respectively. f_s is the force between m_1 and m_2. We then specify

$$x_1 - x_2 = A_0 \sin(\omega t + \gamma) \tag{3.5}$$

$$F_2 = (m_2 + 2m_1)g\mu \tag{3.6}$$

$$F_b = m_b g\mu \tag{3.7}$$

Equation 3.5 is the extent of a swinging smarticle arm as it pushes on the sliding mass. Equation 3.6 is the friction force on a single smarticle, $(m_2 + 2m_1)$ being the mass of one smarticle body and two smarticle arms. Equation 3.7 is the friction force

on the mass that is being pushed on by the smarticle (Either the mass of only the ring or the total mass of the ring and the inactive smarticle). Equations 3.3 and 3.4 can now be solved analytically to find x_1 and $\dot{x}_1$.

$$x_1 = \frac{g(2m_1 + m_2 - m_b)t^2\mu + 2A_0 m_2(\sin(t\omega + \gamma) - \sin(\gamma))}{m_1 + m_2 + m_b} \tag{3.8}$$

$$\dot{x}_1 = \frac{2(g(2m_1 + m_2 - m_b)t\mu + 2A_0 m_2 \omega \cos(t\omega + \gamma)}{m_1 + m_2 - m_b} \tag{3.9}$$

With these equations we can find how far the mass m_b moves before it comes to a stop. The time at which $\dot{x}_1$ is zero defines $t_{\max}$, and the distance that the sliding mass has traveled at that point is $R_{A(B)}$. This distance is R_A or R_B depending on whether we substitute for m_b the mass of just the ring, or the combined mass of the ring and the inactive smarticle. This then allows us to calculate $\langle v_\parallel \rangle$ and $\mathrm{Var}[v_\parallel]$. Plots of all of these quantities along with experimental data are shown in Figure 3.6. Theoretical $\langle v_\parallel \rangle$ is in good agreement with experimental data, and the theoretical $\mathrm{Var}[v_\parallel]$ is accurate for all but very light rings.

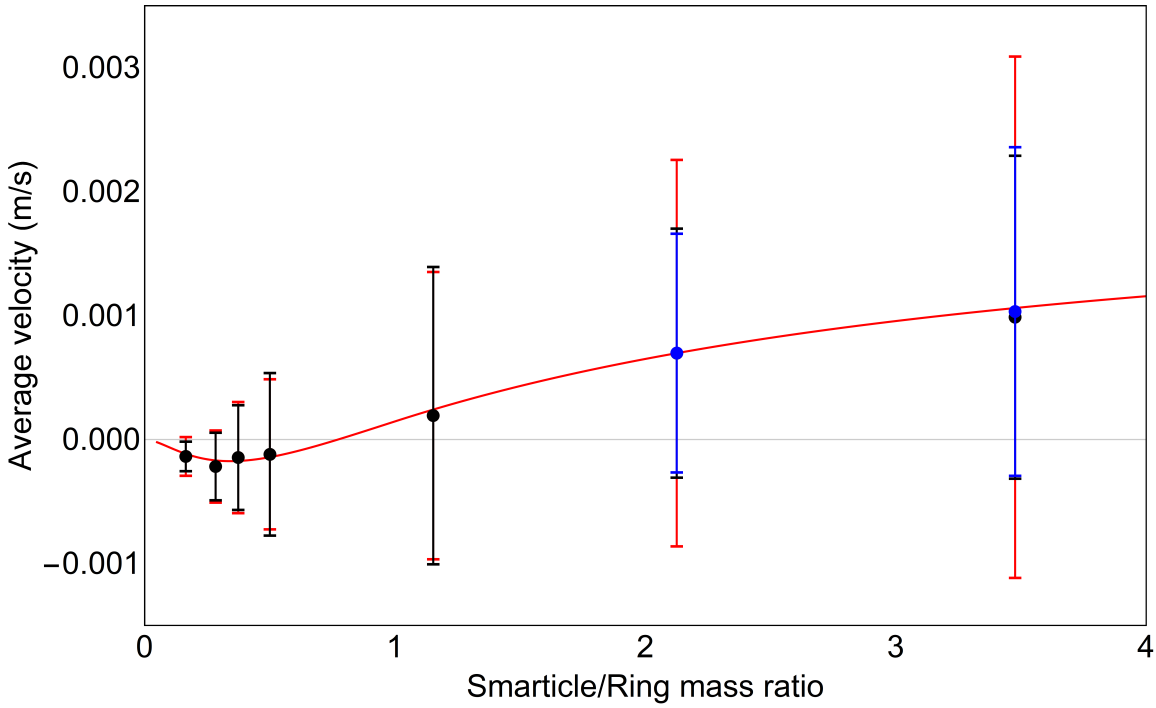

Figure 3.6: **Supersmarticle experiment/theory comparison.** Black is experimental data for supersmarticle system. Red is uncorrelated supersmarticle theory. Blue is Markov chain supersmarticle theory (applied to light ring cases).

To compare the geometric assumption that the probability of nudge type is proportional to the angle swept out by the corresponding section of the ring multiplied by λ or $(1-\lambda)$ we took one trial from the experiment and counted the collision types by hand. The resulting proportion of each collision type is shown compared with the theoretical assumption in Figure 3.7. This is data from the one of the trials from the same data set used in Figure 3.6. It is partial data from one trial that represents 162 collisions over about 50 seconds.

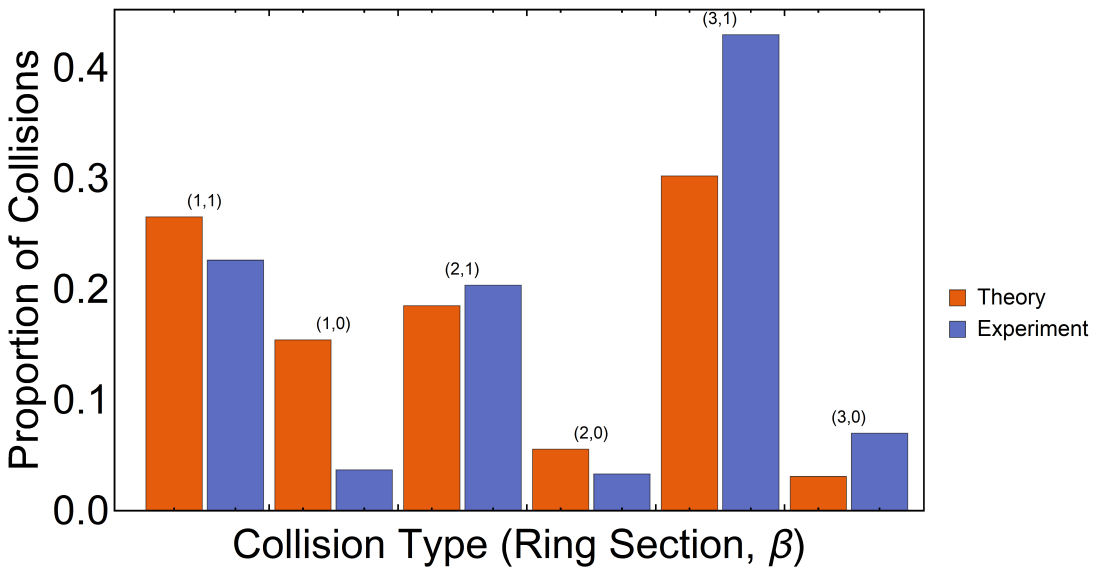

Figure 3.7: Theoretical proportions of each collision type compared with a small sample (half of a single trial) of experimental nudges recorded by hand.

The supersmarticle theory shown above predicts the mean of the directed velocity well, as well as the standard deviation of the velocity when the ring is relatively heavy. The theory begins to fail when it comes to the standard deviation of the velocity of the supersmarticle when the mass of the ring is very light.

3.2.3 Experimental Statistics

The simplest explanation for any discrepancy between theoretical and experimental variance would be the bias introduced by either simple sample variance measurement or the conversion from variance to standard deviation. A good treatment of the ideas of bias and consistency can be found in [41]. Each experimental measurement of the average velocity of the supersmarticle is a sampling of the true distribution of possible average velocities. This average velocity is a random variable in practice because of the delicate nature of the initial conditions of the experiment even if the supersmarticle system is a deterministic dynamical system in principle. In the following section we will describe why statistical bias and inconsistency does not account

for the discrepancy between the previous smarticle theory and experiment.

The simple sample mean from such an experiment is both statistically consistent and unbiased. It is consistent because as the number of samples approaches infinity, the simple sample mean will approach the mean of the true distribution. It is unbiased because treating the sample mean as a random variable itself, the mean of possible realizations of the sample mean is the same as the true distribution mean regardless of the of the number of samples.

$$\begin{aligned}\bar{x} &= \left\langle \frac{1}{N}\sum_i x_i \right\rangle \\ &= \frac{1}{N}\sum_i \langle x_i \rangle \\ &= \mu\end{aligned}$$

where $\bar{x}$ is the sample mean, each x_i is a sample from some probability distribution, N is the number of samples, μ is the true distribution mean, and $\langle \cdot \rangle$ denotes a mean over possible realizations of the enclosed function.

The simple sample variance is consistent but biased.

$$\begin{aligned}\langle \mathrm{Var}[x] \rangle &= \left\langle \frac{1}{N}\sum_i (x_i - \bar{x})^2 \right\rangle \\ = \left\langle \frac{1}{N}\sum_i \left((x_i - \mu) - (\bar{x} - \mu)\right)^2 \right\rangle &= \left\langle \frac{1}{N}\sum_i \left((x_i - \mu)^2 - 2(x_i - \mu)(\bar{x} - \mu) + (\bar{x} - \mu)^2\right) \right\rangle \\ &= \left\langle \frac{1}{N}\sum_i (x_i - \mu)^2 - 2(\bar{x} - \mu)\frac{1}{N}\sum_i (x_i - \mu) + (\bar{x} - \mu)^2 \right\rangle \\ &= \left\langle \frac{1}{N}\sum_i (x_i - \mu)^2 - 2(\bar{x} - \mu)^2 + (\bar{x} - \mu)^2 \right\rangle \\ = \left\langle \frac{1}{N}\sum_i (x_i - \mu)^2 - (\bar{x} + \mu)^2 \right\rangle &= \left\langle \frac{1}{N}\sum_i (x_i - \mu)^2 \right\rangle - \left\langle (\bar{x} - \mu)^2 \right\rangle \\ &= \sigma^2 - \left\langle (\bar{x} - \mu)^2 \right\rangle = \left(1 - \frac{1}{N}\right)\sigma^2\end{aligned}$$

Var[x] is the simple sample variance of x and σ^2 is the true variance of the distribution being sampled. This means that the simple sample variance tends to underestimate the variance of the true distribution by a factor of $\frac{N-1}{N}$. This bias can be corrected by dividing by $N-1$ rather than N. Also, even when the variance is rescaled to be unbiased, the standard deviation is still biased in general because the square root is a concave function and if $f(x)$ is a concave function then $\langle f(x)\rangle \leq f\left(\langle x\rangle\right)$.

$$f(x) \leq f(y) + (x-y)f'(y)$$

Let $x = X$ and $y = \langle X\rangle$.

$$f(X) \leq f(\langle X\rangle) + (X - \langle X\rangle)f'(\langle X\rangle)$$

If we take the expectation of both sides,

$$\langle f(X)\rangle \leq f(\langle X\rangle) + \langle (X - \langle X\rangle)\rangle f'(\langle X\rangle) = f(\langle X\rangle)$$

This concavity means that the simple sample standard deviation which is found by taking the square root of the simple sample variance will underestimate the true standard deviation even when the true variance is estimated in an unbiased way.

The minimum number of trials done with a ring of any mass in this case was 40 which brings the bias in sample variance down to $\sim 2.5\%$. The standard deviation bias is more difficult to estimate, but if the experimental velocities are normally distributed and the above correction is used, then the bias in the standard deviation estimation would be $\sim 1.28\%$. These biases in sample standard deviation do not account for the discrepancy seen in the supersmarticle experimental data versus theoretical prediction.

3.3 Correlations

In the above theory, all nudges are statistically independent. A hypothesis put forward in [2] is that the discrepancy between theory and experiment comes from the neglect of correlations in time between nudges. The independent case does a surprisingly good job modeling the system, especially the mean of the drift, given the strong confinement of the smarticles. Given the success of the previous theory we want to make as small a modification to the previous system as we can in order to improve the weak points of the theory, namely the fluctuations in the drift, without losing what works. Because the original theory is a series of discrete events, it is obvious that the first step in the inclusion of time correlations is the inclusion of single step correlations. We suspect that the correlation times are likely short given the success of the independent theory.

A system where there is some discrete collection of possible states, with each state corresponding to a displacement, and with states independent in time can be characterized by a vector $\mathbf{p}$ where p_i is the probability of choosing state i and a vector $\mathbf{r}$ where r_i is the displacement resulting from choosing state i. If X is the total displacement after N steps, μ_X is the mean of X, and σ_X^2 is the variance of X ,

$$\mu_X = \left\langle \sum_i^N x_i \right\rangle = N \langle x_i \rangle = N(\mathbf{r} \cdot \mathbf{p}) \tag{3.10}$$

$$\sigma_X^2 = \mathrm{Var}\left[\sum_i^N x_i\right] = N\mathrm{Var}[x_i] = N[(\mathbf{r} \circ \mathbf{r} \cdot \mathbf{p}) - (\mathbf{r} \cdot \mathbf{p})^2] \tag{3.11}$$

where $(\circ)$ denotes element-wise multiplication.

3.3.1 Markov Process

To include short time correlations, we vary the probability distribution of the next chosen state dependent on the current state. This takes the system from a series of states taken from a stationary probability distribution to a series of states taken from a finite Markov process, where the probability of each collision type depends on the previous collision.

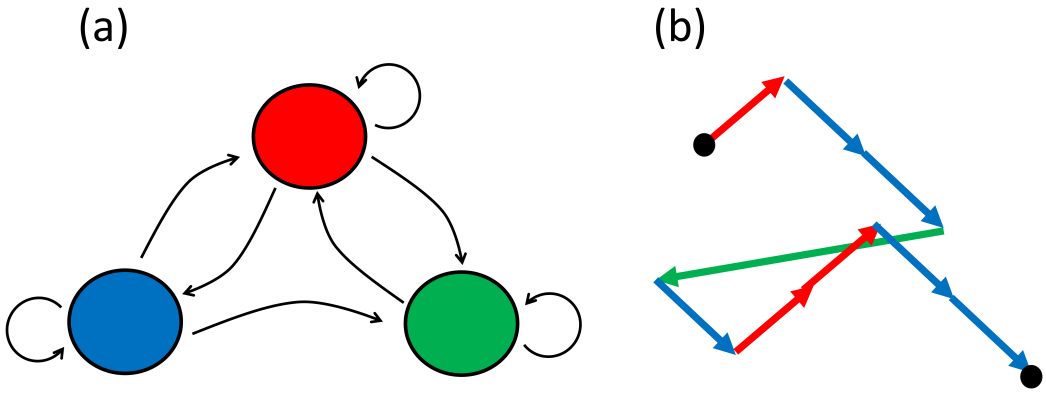

Figure 3.8: **Cumulative Markov chain.** (a) An illustration of a 3 state discrete Markov system with each possible state a different color. (b) An example realization of displacements from such a system.

This system with N states can be characterized by the triple $\{\mathbf{T}, \mathbf{r}, \mathbf{p_0}\}$ where T_{ij} is the probability of transition from state j to state i, r_i is the displacement corresponding to state i, and p_{0i} is the initial probability for the system to be in state i [42]. $\mathbf{T}$ can act on $\mathbf{p_0}$ from the left to give the probability of the state of the system at the next time step, so $\mathbf{T}^n\mathbf{p_0}$ is the probability distribution over the states of the system at time step n. $\mathbf{T}$ has a number of eigenvectors $\mathbf{u}_i$ equal to the number of states of the system with corresponding eigenvalues $\lambda_i \leq 1$ with exactly one eigenvalue equal to 1. As the number of time steps approaches infinity, the probability distribution $\mathbf{p}_t$ over the states of the system will settle down to a steady

state equal to the normalized eigenvector of $\mathbf{T}$ corresponding to a eigenvalue of 1. A simple example of such a system is illustrated in Figure. 3.8. The colored circles are different states of the system. The black arrows represent the transition probabilities between the states. The colored arrows show the path taken by accumulating the displacements from the state diagram.

3.3.2 Intermediate Time Statistics

We are interested in the intermediate behavior of the system after a large number of steps, but not so many that the system has reached its steady state ($1 \ll e^N < e^{\lambda_2}$ where λ_2 is the largest eigenvalue less than 1). Calculations in this regime become cumbersome because they involve large numbers of matrix multiplications. Instead, we write the mean μ_X and mean of the square $\langle X^2 \rangle$ of the sum of displacements in terms of the eigenvalues and eigenvectors of $\mathbf{T}$ and the matrix of right eigenvectors $\mathbf{U}$ such that U_{ij} is the jth components of the ith eigenvector.

$$\mu_X = \sum_n \mathbf{U}^{\intercal\text{-}1}\mathbf{p_0} \circ \boldsymbol{\lambda}^{\circ n}\mathbf{U} \cdot \mathbf{r} \tag{3.12}$$

$$\left\langle X^2 \right\rangle = 2\sum_{m<n} \mathbf{U}\mathbf{r} \circ \boldsymbol{\lambda}^{\circ(n-m)}\mathbf{U}^{\intercal^{-1}} \circ \mathbf{r}\mathbf{U}^{\intercal} \circ \boldsymbol{\lambda}^{\circ m}\mathbf{U}^{\intercal^{-1}} \cdot \mathbf{p_0} + \sum_m \mathbf{U}\mathbf{r}^{\circ 2} \circ \boldsymbol{\lambda}^m \mathbf{U}^{\intercal^{-1}} \cdot \mathbf{p_0} \tag{3.13}$$

The derivation of these formulas can be found below. Denoting each displacement as x_n and the sum of those displacements as X we calculate the mean of the sum of the displacements μ_X.

$$\mu_X = \left\langle \sum_n x_n \right\rangle = \langle x_1 + x_2 + \cdots x_N \rangle$$

We write the average of each displacement as the possible displacements weighted

by the probability that displacement x_n has value r_i.

$$\mu_X = \sum_{n,i} r_i P(x_n, i)$$

In terms of unit vectors e_i, transition matrix $\mathbf{T}$, and initial probabilty vector p_0 this becomes

$$\mu_X = \sum_{n,i} \langle e_i|r\rangle \, \langle e_i|\mathbf{T}^n|p_0\rangle$$

Next, we put p_0 in the eigenbasis of $\mathbf{T}$ using the right eigenvectors u_k (because we will be acting with $\mathbf{T}$ from the left).

$$\mu_X = \sum_{n,i} \langle e_i|r\rangle \, \langle e_i|\mathbf{T}^n \sum_k |u_k\rangle\langle e_k|\mathbf{U}^{\intercal\text{-}1}|p_0\rangle$$

We can now replace powers of $\mathbf{T}$ acting on eigenvectors with powers of eigenvalues multiplying eigenvectors.

$$\mu_X = \sum_{n,i} \langle e_i|r\rangle \, \langle e_i| \sum_k \lambda_k^n |u_k\rangle\langle e_k|\mathbf{U}^{\intercal\text{-}1}|p_0\rangle = \sum_{n,i,k} \lambda_k^n \, \langle e_i|r\rangle \, \langle e_i|u_k\rangle\langle e_k|\mathbf{U}^{\intercal\text{-}1}|p_0\rangle$$

Writing this in component form,

$$\mu_X = \sum_{n,i,k} \lambda_k^n r_i U_{ki} \sum_l U_{kl}^{\intercal\text{-}1} p_{0l} = \sum_{n,i,k,l} \lambda_k^n r_i U_{ki} U_{kl}^{\intercal\text{-}1} p_{0l}$$

and converting back to vector notation,

$$\mu_X = \sum_n \mathbf{U}^{\intercal\text{-}1}\mathbf{p_0} \circ \boldsymbol{\lambda}^{\circ n}\mathbf{U} \cdot \mathbf{r} \tag{3.14}$$

where $\boldsymbol{\lambda}$ is the vector of eigenvalues of $\mathbf{T}$ and $\boldsymbol{\lambda}^{\circ n}$ is element-wise multiplication of $\boldsymbol{\lambda}$ by itself n times. Next, in order to compute the variance of the displacement we calculate the second statistical moment of the total displacement.

$$\left\langle X^2 \right\rangle = \left\langle \left(\sum_n x_n \right)^2 \right\rangle = \left\langle (x_1 + x_2 + \cdots x_N)^2 \right\rangle$$

$$= \left\langle x_1^2 + x_1 x_2 + \cdots x_1 x_N + x_2 x_1 + x_2^2 + \cdots x_2 x_N + \cdots x_n^2 \right\rangle = \sum_{n,m} \langle x_n x_m \rangle$$

We replace the average of $x_n x_m$ with the values of their displacements weighted by the probability of each of the nudges having those displacements.

$$\left\langle X^2 \right\rangle = \sum_{n,i,j} r_i r_j P\left((x_n, i) \cap (x_m, j)\right)$$

$P\left((x_n, i) \cap (x_m, j)\right)$ can be read as the probability that displacement n has a value of r_i and displacement m has a value of r_j. We split the sum over m into three parts; one where $m < n$, one where $m > n$, and one where $m = n$.

$$\left\langle X^2 \right\rangle = \sum_{m<n,ij} r_i r_j P\left((x_n, i) \cap (x_m, j)\right)$$
$$+ \sum_{n<m,ij} r_i r_j P\left((x_n, i) \cap (x_m, j)\right) + \sum_{m=n,ij} r_i r_j P\left((x_n, i) \cap (x_m, j)\right)$$

The first two sums are identical under the exchange of m and n so they can be contracted into a single term.

$$\left\langle X^2 \right\rangle = 2 \sum_{m<n,ij} r_i r_j P\left((x_n, i) \cap (x_m, j)\right) + \sum_{m=n,ij} r_i r_j P\left((x_n, i) \cap (x_m, j)\right)$$

Then, we replace the joint probability of the two particular displacements having particular values with the probability of the value of the later displacement given the value of the earlier displacement multiplied by the probability of the earlier displacement having a particular value.

$$\left\langle X^2 \right\rangle = 2 \sum_{m<n,ij} r_i r_j P\left((x_n, i) | (x_m, j)\right) P\left(m, j\right) + \sum_{m=n,ij} r_i r_j P\left((x_n, i) | (x_m, j)\right) P\left(m, j\right)$$

$P\left((x_n, i)|(x_m, j)\right)$ can be read as the probability of displacement n having value r_i given that displacement m has value r_j. In terms of unit vectors e_i, transition matrix $\mathbf{T}$, and initial probability vector p_0 this becomes

$$\begin{aligned}\left\langle X^2\right\rangle = 2 \sum_{m<n,i,j} \langle e_i|r\rangle \langle r|e_j\rangle \left\langle e_i|\mathbf{T}^{n-m}|e_j\right\rangle \langle e_j|\mathbf{T}^m|p_0\rangle \\ + \sum_{m,i,j} \langle e_i|r\rangle \langle r|e_j\rangle \underbrace{\left\langle e_i|\mathbf{T}^{m-m}|e_j\right\rangle}_{\delta_{ij}} \langle e_j|\mathbf{T}^m|p_0\rangle\end{aligned}$$

We then write everything in the eigenbasis of $\mathbf{T}$ using eigenvectors u_k and the matrix of eigenvectors $\mathbf{U}$.

$$\begin{aligned}\left\langle X^2\right\rangle = 2 \sum_{m<n,i,j} \langle e_i|r\rangle \langle r|e_j\rangle \langle e_i|\mathbf{T}^{n-m} \sum_k |u_k\rangle\langle e_k|\mathbf{U}^{\intercal^{-1}}|e_j\rangle\langle e_j|\mathbf{T}^m \sum_l |u_l\rangle\langle e_l|\mathbf{U}^{\intercal^{-1}}|p_0\rangle \\ + \sum_{m,i} \langle e_i|r\rangle^2 \langle e_j|\mathbf{T}^m \sum_k |u_k\rangle\langle e_k|\mathbf{U}^{\intercal^{-1}}|p_0\rangle\end{aligned}$$

This allows us to replace powers of $\mathbf{T}$ with powers of its eigenvalues λ_k.

$$\begin{aligned}\left\langle X^2\right\rangle = 2 \sum_{m<n,i,j} \langle e_i|r\rangle \langle r|e_j\rangle \langle e_i| \sum_k \lambda_k^{n-m}|u_k\rangle\langle e_k|\mathbf{U}^{\intercal^{-1}}|e_j\rangle\langle e_j| \sum_l \lambda_l^m|u_l\rangle\langle e_l|\mathbf{U}^{\intercal^{-1}}|p_0\rangle \\ + \sum_{m,i} \langle e_i|r\rangle^2 \langle e_j| \sum_k \lambda_k^m|u_k\rangle\langle e_k|\mathbf{U}^{\intercal^{-1}}|p_0\rangle\end{aligned}$$

$$\begin{aligned}\left\langle X^2\right\rangle = 2 \sum_{m<n,i,j,k,l} \lambda_k^{n-m}\lambda_l^m \langle e_i|r\rangle \langle r|e_j\rangle \langle e_i|u_k\rangle\langle e_k|\mathbf{U}^{\intercal^{-1}}|e_j\rangle\langle e_j|u_l\rangle\langle e_l|\mathbf{U}^{\intercal^{-1}}|p_0\rangle \\ + \sum_{m,i,k} \lambda_k^m \langle e_i|r\rangle^2 \langle e_j|u_k\rangle\langle e_k|\mathbf{U}^{\intercal^{-1}}|p_0\rangle\end{aligned}$$

Writting this is component form,

$$\left\langle X^2\right\rangle = 2 \sum_{m<n,i,j,k,l,q} \lambda_k^{n-m}\lambda_l^m r_i r_j U_{ki} U^{\intercal^{-1}}_{kj} U_{lj} U^{\intercal^{-1}}_{lq} p_{0q} + \sum_{m,i,k,q} \lambda_k^m r_i^2 U_{ki} U^{\intercal^{-1}}_{kq} p_{0q}$$

an converting back to vector notation,

$$\left\langle X^2 \right\rangle = 2 \sum_{m<n} \mathbf{U}\mathbf{r} \circ \boldsymbol{\lambda}^{\circ(n-m)} \mathbf{U}^{\intercal^{-1}} \circ \mathbf{r}\mathbf{U}^{\intercal} \circ \boldsymbol{\lambda}^{\circ m} \mathbf{U}^{\intercal^{-1}} \cdot \mathbf{p_0} + \sum_{m} \mathbf{U}\mathbf{r}^{\circ 2} \circ \boldsymbol{\lambda}^{m} \mathbf{U}^{\intercal^{-1}} \cdot \mathbf{p_0} \tag{3.15}$$

This formulation involves powers of the λ_i rather than powers of $\mathbf{T}$ and allows for much faster exact calculation.

3.3.3 Correlations and Variance

Correlations in time have a strong effect on the variance of sum realizations. The most extreme values of sums are always going to involve choosing the same state repeatedly, so if the probability of choosing the same state consecutively is changed, then the probabilities of extreme values for the sum are disproportionately affected. When repeating the same state is more probable so are extreme values for the sum, and when repeating the same state is less probable, the extreme values for the sum are less probable.

Two state system

As a simple example we begin with a one-dimensional case of two states a and b with displacements $r_a = 1$ and $r_b = -1$.

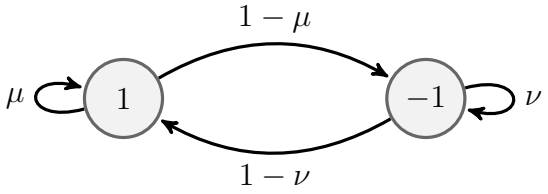

Figure 3.9: **2 state system.** A diagram of a two state Markov chain with $r = (1, -1)$ and probabilities parametrized by μ and ν.

We can then use the values of μ and ν to control the one step correlations in

the system. When the values of μ and ν are close to 1 we will say that the system has positive correlation in time, and when they are close to 0 we will say that the system has negative correlation. In order to enforce a one-dimensional transition from negative to positive correlation, we constrain the mean to be constant. For example, if we constrain μ and ν such that the mean of the sum of displacements is 0 then in the limiting case of high positive correlation, the variance of the sum of displacements goes to 0. This is because in the limit of small μ and ν the system becomes deterministic and jumps back and forth between 1 and -1, so every sum of displacements can only be 1 or -1 if N is odd, or 0 if N is even. In the limit of high positive correlation the possible sums are reduced to only the two extreme possibilities, N and $-N$, and the variance becomes maximized to N^2.

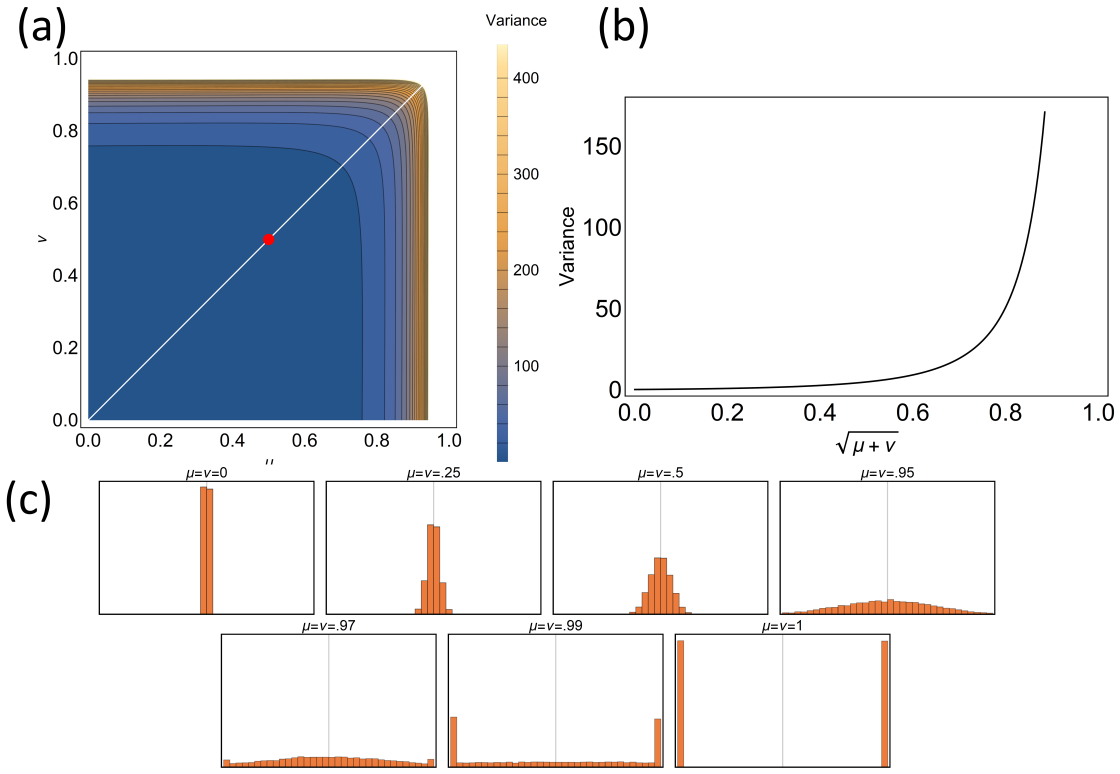

Figure 3.10: **2 state sum distributions.** (a) $\mu - \nu$ parameter space white line is constant mean of 0. The red dot corresponds to all states having equal probability every step. (b) Variance versus autocorrelation ($\sqrt{\mu^2 + \nu^2}$) along 0 mean contour. (c) The evolution of the distribution of sums as correlation parameters as changed. $N = 100$

Notice how the histogram evolves as we move from negative to positive correlation (Figure 3.10c). With negative correlations we have a unimodal distribution of possible sums, but as the the system moves to more positive correlations, it approaches a bimodal distribution. When $\mu = \nu = \frac{1}{2}$ we get a normal distribution over sums because the distribution over states is identical, so the central limit theorem is exact. When the correlations are strongly negative, the distribution for every step is no longer identical, but the distribution of possible displacements over windows of two time steps is nearly identical, so the system approximately converges to a Gaussian. However, when the correlations are strongly positive, the distribution over states is significantly modified by which state is chosen first. The limiting cases for the distribution of X in $\mu - \nu$ space with $r = (a, b)$ are

$$P(X) = \begin{cases} \delta(X - \frac{N}{2}(a+b)), & \mu = \nu = 0 \\ \mathcal{N}(\frac{N}{2}(a+b), \frac{N}{2}((1-\mu)(1-\nu))(a+b)^2 - \frac{(a+b)^2}{2}), & \mu, \nu \ll 1 \\ \mathcal{N}(\mu_X, \sigma_X^2), & \mu = \nu = \frac{1}{2} \\ \frac{1}{2}(\delta(X-a) + \delta(X-b)), & \mu = \nu = 1 \end{cases} \tag{3.16}$$

where only leading order terms have been included where approximations are made.

Three state system

If we extend the system to more than two states, then we expect correlations to have a similar effect. In the limit of high positive correlation, the variance still increases with more negative correlation.

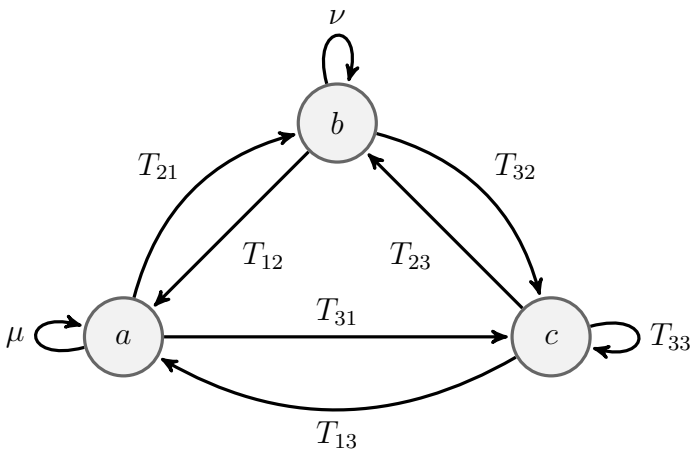

Figure 3.11: **3 state system.** A diagram of a three state markov chain with $r = (a, b, c)$ and probabilities $\mathbf{T}$ parametrized by μ and ν.

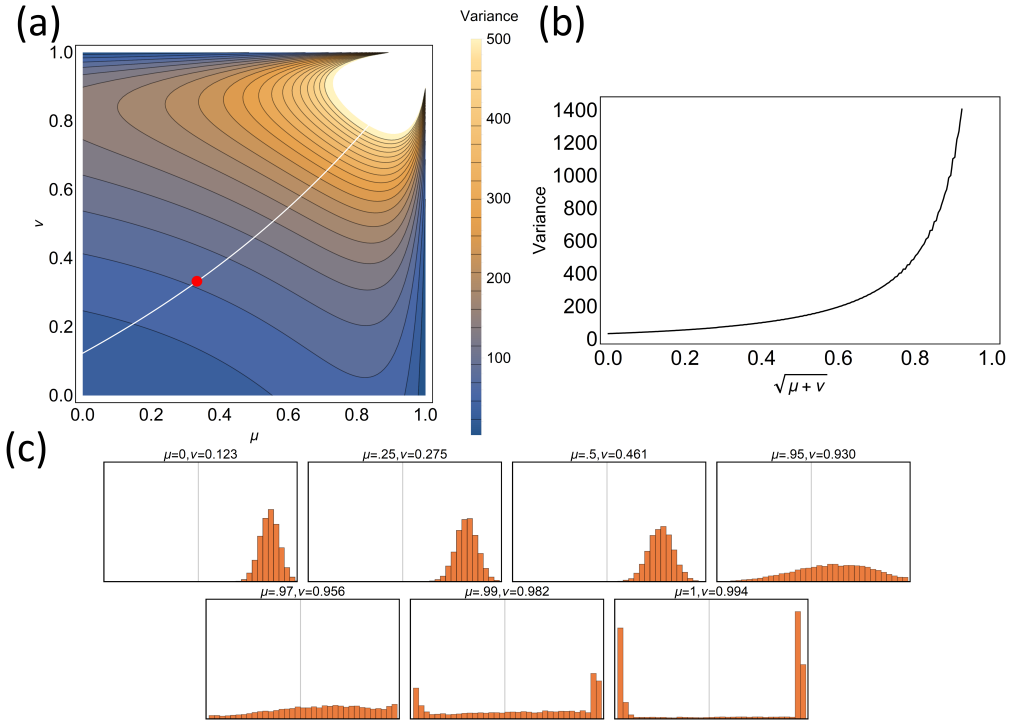

Figure 3.12: **3 state sum distributions.** (a) $\mu - \nu$ parameter space. The white line is the contour of constant mean of $\frac{1}{3}(1 - 1 + \frac{1}{2})$. The red dot corresponds to all states having equal probability every step. (b) Variance versus autocorrelation ($\sqrt{\mu^2 + \nu^2}$) along $\frac{1}{3}(1 - 1 + \frac{1}{2})$ mean contour. (c) The evolution of the distribution of sums as correlation parameters as changed. $r = (1, -1, \frac{1}{2})$, $N = 100$

Exact statements about the produced distributions become harder to make than in the two-state system because the constraints on the system are much weaker but the same patterns persist. The large magnitude sums still involve repeating the largest magnitude state many times in a row, so if the ability of the system to repeat its short-term behavior is diminished then the variance will decrease.

Markov Supersmarticles

Applying this idea to the supersmarticle, we identify each state of the Markov chain with a section of the supersmarticle ring (Figure 3.3(b)) including splitting the disjoint section 2 into two distinct states. We also differentiate between the inactive smarticle being in contact with the ring or not to make a total of 8 states. For each state, the displacements from a nudge remain the same as they did before, and the direction is the average of θ over the corresponding section of the ring. The probability of a nudge in the direction of a section of the ring is the fraction of the ring that section covers. Using this formulation, the mean displacement of the ring is unchanged from the continuous angle system.

When the ring is light, it can move a significant distance with a single nudge. This movement causes subsequent nudges to be less likely to act on the same part of the ring. This is supported by the data shown in Figure 3.13. With this in mind we modify the transition matrix in the cases where the ring is significantly lighter than a single smarticle,

$$\mathbf{T}' = \mathbf{Z} \circ \mathbf{T} \tag{3.17}$$

$$Z_{ij} = \begin{cases} \mu & \text{if nudge i and j are in the same direction} \\ 1 & \text{otherwise} \end{cases}$$

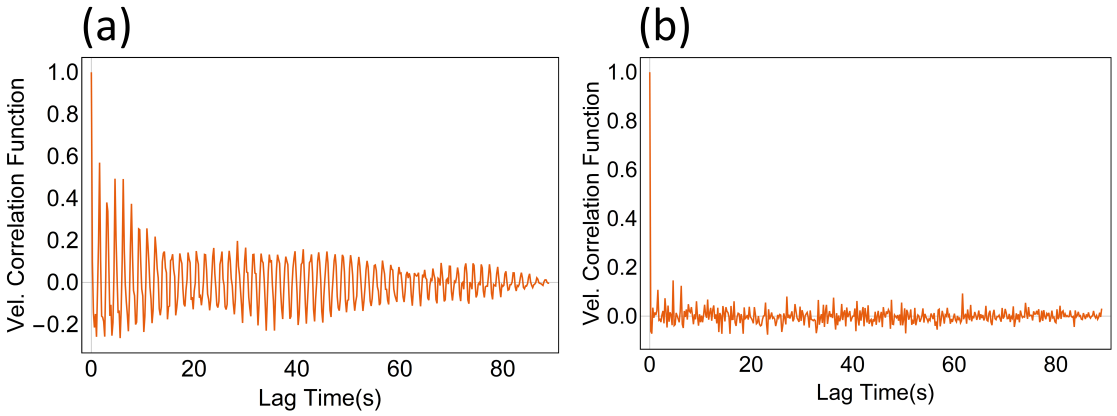

Figure 3.13: **Correlation functions of $v_{\parallel}$.** (a) The correlation function of $v_{\parallel}$ of an experimental trial of the lightest ring. (b) The correlation function of $v_{\parallel}$ of an experimental trial of the heaviest ring.

and then re-normalize the columns of $\mathbf{T}'$ and fit the mean with λ the same as in the uncorrelated case. Using a value of $\mu < 1$, we make consecutive nudges in the same direction less likely. When the system has high negative correlation in nudge direction ($\mu \ll 1$) the standard deviation of the velocity of the supersmarticle is very close to the experimental value (Figure 3.6).

3.3.4 State space vs. physical space

A situation that can be misleading when considering this theory is if physically distinct states produce identical displacements. In this case there could be high negative correlations in a physical sense but less so in terms of the possible displacements. For example, consider the hypothetical case of an accumulation of charged particles one by one and we are interested in the total charge of the accumulation after some time. Particle A has a charge of q_1, particle B also has a charge of q_1, and particle C has a charge of q_2. The corresponding Markov diagram would be

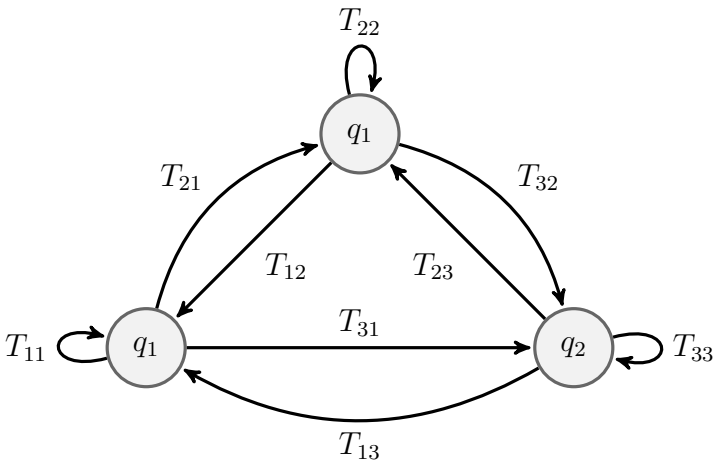

Figure 3.14: **3 state physical system.** A diagram of a three state markov chain with $r = (q_1, q_1, q_2)$ and transition matrix $\mathbf{T}$.

The above theory would naively predict that if you are very likely to accumulate the same type of particle most recently seen then the variance of total charge would be high and if you are very unlikely to see the same particle type twice in a row than the variance of total charge would be low. However, the above diagram is reducible to

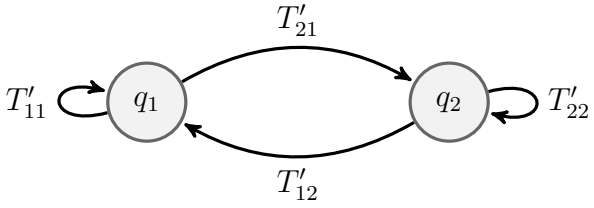

Figure 3.15: **Equivalent 2 state system.** A diagram of a two state Markov chain with $r = (q_1, q_2)$ and transition matrix $\mathbf{T}'$.

where

$$T'_{11} = T_{11} + T_{22} + T_{12} + T_{21} \tag{3.18}$$

$$T'_{21} = T_{32} + T_{31} \tag{3.19}$$

$$T'_{12} = T_{13} + T_{23} \tag{3.20}$$

$$T'_{22} = T_{33} \tag{3.21}$$

Because the charge added by two different particle types is the same, their two nodes in state space can be combined. The transition probabilities going to and from the new node are sums of the probabilities that give the same charge outcome. These new probabilities are can be very different than the original ones so it is important to make a distinction between physical correlations in an experimental system and the correlations in the Markov system because strong negative correlations in a physical sense does not necessarily mean the same is true in the Markov system. For this reason, it is important to work with the maximally reduced Markov graph.

3.4 Discussion

Smarticles are different from the typical robotic ensemble[43, 44] in that they were deliberately designed without high functionality or top down control. They are not controlled through a process whereby every robot is told what to do from a central computer and they do not communicate between each other. Instead they can respond to their environment in softer ways such as listening for a tone, or looking for light. The supersmarticle is more similar to a moving bacteria [45], swimming algae [46] or slime mold [47] rather than a group of aware agents like ants [48] or birds [49]. Following [50] they are classified as a non-cooperative, unaware, non-coordinated, distributed multi robot system. This is the lowest level of cooperation, knowledge, coordination, and organization in robotic swarms. These attributes are

also the reason that the system in general has such short correlation times that allow the use of a random process to model the system.

The application of the Markov chain theory in this chapter could have application in controlling diffusing systems. For instance, some tasks could require very rapid diffusion while another could require very precise movement. One task that could require rapid diffusion would be exploration of a space. If a group of robots wanted to cover a large unknown area in a short amount of time, it could be advantageous for each robot to pick a direction and repeatedly step in the that direction over and over. This would allow the robots to cover a larger exploratory area in a short amount of time, at the expense of precision. In the context of the above theory this is the regime of high positive correlations. However, if the robots have a known goal location, that requires a precision path to get to, it could be better to take smaller steps and follow a "two steps forward, one step back" sort of protocol. This would allow for lower fluctuations in their movement because the robots would be firmly in the negative correlation regime.

One example of natural creatures who exhibit this type of motion are algae [51]. There are certain very species of algae that move by swimming with a set of four flagella. Through a genetic difference some of them swim with a four-fold synchronized jellyfish style motion that results in a back and forth motion with slow but steady progress, while some of them swim by alternating pairs of flagella resulting in rapid movement in one direction. The existence of both of these behaviors could suggest that the negatively correlated motion of the jellyfish style swimming and the positively correlated motion of the alternating flagella swimming could be more useful in different environments or situations.

Future of smarticles

There are two different directions that the engineering of smarticles can go from here. First, they can be made "smarter" by giving more sophisticated control, computational power, or communication. They can be tailored to more specific tasks than locomotion like getting through mazes [2], foraging [52, 53], or transportation of objects [54]. This will lead to a more traditionally engineered robot that is more effective at a small set of tasks. Alternatively, the simplicity of the elements can be maintained, but the elements can be reduced in size and/or increased in number. This would lead to an active material with micro- or nano-bot elements who might control the properties of the material through their geometry similar to [55]. It is the opinion of the author that the latter is a more interesting path. The simplicity of the smarticles is their strength and their surprising variety of behaviors (pair gliders, regular patterns, directed diffusion) and control options (sound-based, phototaxis) despite their relatively unsophisticated design is where they excel.

3.5 Summary

We have developed a kinetic theory of supersmarticles and explained the change in direction of the supersmarticles average velocity as a function of the mass of the enclosing ring. We have made quantitative statements about the mean and variance of the velocity of the supersmarticle that match with experimental data. By extending the theory to include short time correlations we have been able to plausibly explain the change in fluctuation size of the supersmarticles velocity as a function the mass of the ring.

Chapter 4
Fluctuation Feedback in Complicated Systems

4.1 Introduction

In a recent paper by Chvykov and England [3] a general treatment for dynamical systems with widely separated time scales was shown. They contend that a wide range of many-body systems exhibit time scale separation in their dynamics or there is a macroscopic order parameter that can be treated as varying on a slower time scale than the rest of the system. This work served as an early inspiration for the proceeding work and so we start by briefly describing their results here. We will then explore the consequences and validity of these results through a small number of concrete examples that illuminate some aspects of the theory. Our examples will show that there is usefulness in thinking about a certain class of systems in this way. The system in question is one where different members evolve on different time scales, identified as fast variables and slow variables. There are two components to their result. First, we can approximate the dynamics of the slow variables with an average drift and noisy fluctuations rather than following all of the detailed dynamics of the fast variables. Second, that the effect of inhomogeneous noise is qualitatively similar to a weak attraction to low noise amplitude regions. The fast and slow variables are functions of each other in that the dynamical equations for the fast variables contain the slow variables and vice versa. The short time details of the fast variables' motion become unimportant because the slow variables react on a longer time scale. The fast variables are then treated as noise from the point of view of the slow variables. From

the fast variable's point of view the slow variable is treated as constant. Starting from

$$\eta \dot{x}_a = F_a(x_a, y_i, t) + \sqrt{2T\eta}\xi_a \tag{4.1}$$

$$\mu \dot{y}_i = f_i(x_a, y_i, t) + \sqrt{2T\mu}\xi_i \tag{4.2}$$

with the x_a as the slow variables and the y_i as the fast variables and the ξ are Gaussian white noise the resulting dynamics of the slow variable are

$$\gamma_{ab} \cdot \dot{x}_b = \epsilon \langle F_a \rangle_{y|\text{fix } x} + \sqrt{2\epsilon D_{ab}} \cdot \xi_b \tag{4.3}$$

$$\gamma_{ab}(x) = \delta_{a,b} + \epsilon \int \mathrm{d}t'(t - t') \langle i\tilde{y}\partial_b f_i|_{t'}, F_a|_t \rangle_{y|\text{fix } x} \tag{4.4}$$

$$D_{ab}(x) = T\delta_{a,b} + \frac{\epsilon}{2} \int \mathrm{d}t' \langle F_a|_{t'}, F_b|_t \rangle_{y|\text{fix } x} \tag{4.5}$$

with $\epsilon = \mu/\eta \ll 1$. Equation 4.3 is similar to the original equation for the evolution of x_a with a deterministic term and a noise term. The new force term is the average of the original dynamical function for the slow variables over the steady state of the fast variables with fixed slow variables. The new noise term is similar to the original from Equation 4.1 with the magnitude of the noise increased in a non-trivial way by the motion of the fast variables. In an effort to be general, the authors used an approach that lead to a result that is not easily applicable to specific cases. The second term in Equation 4.4 can be intractable because of the inclusion of $\tilde{y}$ which is a "response field" which arises from the functional integrals used in the derivation of this formula. This field is only known analytically for a small number of special cases although it can be argued that it is a negligible term when the correlation time of the effect on the slow variables from the fast variables is very short. Overall, this formulation gives an approximation to the slow dynamics that only depends on steady state means and the intermediate time fluctuations of the system. The second term

in Equation 4.5 is how the magnitude of noise is modified by the motion of the fast variables once again averaging the motion of the fast variables over the steady state with fixed slow variables. The result is a competition between the effects of an average force $\langle F(x) \rangle$ and an in general inhomogeneous effective temperature landscape. By temperature landscape we mean that there are some places in the space of the slow variables where the magnitude of effective noise from the motion of the fast variables is larger or smaller. An important detail is that the effect of the average force is generically much stronger because it is of order ϵ while the effect on the slow variable from inhomogeneous noise is of order ϵ^2.

An example of this kind of approximation is when we use random noise to model the motion of Brownian particles [56]. In this case the model consists of a comparatively large particle being moved by a series of collisions by a bath of smaller particles. We can model this motion with a series of collisions which are independent of one another and the motion of the Brownian particle amounts to a random walk. Here, we do not contend that the motion of any constituent of the system is actually random. We still believe that the motion of the particle being followed and the surrounding medium is in principle an exactly deterministic system where every member could be followed from exact initial conditions. We use random walks and stochastic processes to model the motion because the correlation times at the resolution we practically measure for such a system are so short that it is effectively a random process from the point of view of an experiment. If we are interested in the dynamics of a system where some of elements have much shorter correlation times than others, then it could make sense to treat the effects of those elements as noise in a similar way.

4.2 Episodic behavior

If the collection of trajectories representing the dynamics of the system can be coarse grained into multiple distinct possible behaviors and amplitude of noise is

large enough to jump between macroscopic patterns in the deterministic dynamics, then the system can be treated statistically. The system will spend irregular intervals of time exhibiting a pattern of behavior before switching to another. Also, the system will tend to spend a longer time in patterns with lower amplitude fluctuations before switching to another. For example, imagine that one of the behaviors that a system could exhibit was exactly periodic. This would mean that the fluctuations of this behavior are zero and the system would continue in that pattern indefinitely. However, if a pattern of behavior was only nearly periodic, then it would take some time for the system to drift and the system would spend a long time exhibiting a similar pattern.

4.2.1 Potential with Inhomogeneous Noise

Before we look at examples of systems that can be approximated with average drift and noise, we examine the behavior of a system which is explicitly defined as such. We use a simple example of a particle in a double well potential with some dissipation.

$$\ddot{x} = ax(-x^2 + 8) + b\xi - c\dot{x} \tag{4.6}$$

where ξ is gaussian white noise. Without noise ($b = 0$), the particle settles into the minimum of one of the wells, choosing its final state depending on its initial position and velocity. By including constant Gaussian white noise to the system, the particle alternates spending time in each well episodically before jumping to the other. If we then add a gradient so that the amplitude of the noise is lower in one of the wells than the other we see that the system spends most of its time in the lower noise well, only making short excursions into the other.

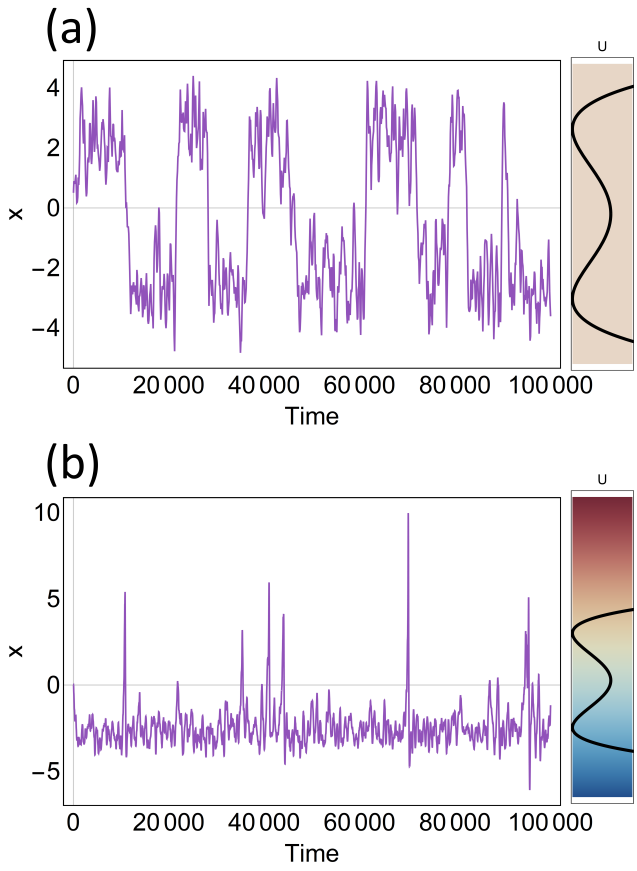

Figure 4.1: **Effect of noise gradient.** The movement of a particle subject to Equation 4.6. The trajectory x of the particle is shown on the left in purple. On the right the potential is shown as a curve and the magnitude of the noise is shown as a gradient with blue being lower amplitude and red being higher. (a) The trajectory of a particle subject to the double well potential shown with uniform noise amplitude. The particle spends time in each well before being kicked to the other. (b) The trajectory of a particle subject to the same potential well, but now there is a gradient to the magnitude of the noise with blue being lower amplitude and red being higher amplitude. The particle spends almost all of its time in the well with the lower amplitude noise, only making short excursions into the other well. The parameter values used are $a = 4 \times 10^{-6}$, $b = 1 \times 10^{-2}$, $c = .01$.

If the noise is too weak, then we are closer to the deterministic regime and the particle basically does what would be expected from just the potential with a little noise added. If the noise is too strong then the particle doesn't spend any extended time in either well and diffuses while basically ignoring the potential. The regime

shown here is one where both noise and potential are important, and their competing forces lead to episodic behavior with a preference for lower amplitude noise states.

4.3 Lorenz equations

As an example of a system with a separation of time scales, we will explore the Lorenz equation with a slowly varying parameter. This system is a good choice for such a study because it is a highly chaotic system, so correlation times are short. Even better, its trajectories all pass through a region with a high local Lyapunov exponent repeatedly, so trajectories spread through the attractor quickly [57]. The macroscopic state or overall behavior of the system is parametrized by the slow varying parameter ρ. There is a feedback where value of the slow variable dictates the distribution of trajectories of the faster variables, and the behavior of the faster variables determines the dynamics of the slow variable. There are some situations where this feedback can cause the parameter to stall near a particular value even if the system does not find a stationary point. If the distribution of possible trajectories of the fast variables are centered around a stationary point of the slow variable, the average drift is zero. If the fluctuations away from the stationary point due to different trajectories of the fast variables are small, then the slow variable will stall there until a large enough fluctuation occurs to change the behavior of the system.

4.3.1 Fixed ρ behaviors

To build an example of this class of system we begin with the Lorenz equations [58].

$$\dot{x} = \sigma(y - x) \tag{4.7}$$

$$\dot{y} = x(\rho - z) - y \tag{4.8}$$

$$\dot{z} = xy - \beta z \tag{4.9}$$

The following summary of the systems behavior as ρ is varied is adapted from [59]. There are in general 3 stationary points, the origin $(0, 0, 0)$, C_1 $(+\sqrt{\beta(\rho-1)}, +\sqrt{\beta(\rho-1)}, \rho-1)$, and C_2 $(-\sqrt{\beta(\rho-1)}, -\sqrt{\beta(\rho-1)}, \rho-1)$. Both C_1 and C_2 are symmetric about the z axis. The stability of these stationary points changes as we vary ρ. Their stability is summarized in Table 4.1

Table 4.1: The stability of the stationary points of the Lorenz system. At $r = \frac{470}{19} \approx 24.74$ C_1 and C_2 lose their stability in a subcritical Hopf bifurcation.

Interval	Origin Stability	C_1 and C_2 Stability
$0 < \rho < 1$	Stable	Unstable
$1 < \rho < 24.74...$	Unstable	Stable
$24.74... < \rho$	Unstable	Unstable

In the chaotic regime of the Lorenz system the trajectory forms the familiar butterfly shape shown in Figure 4.2 ($\rho = 25$). This is caused by the trajectory orbiting C_1 and C_2 in a chaotic manner. The orbits around C_1 form one lobe and the orbits around C_2 form the other. The distribution of possible numbers of orbits before switching lobes is not constant with ρ. For instance, when $\rho = 28$ the maximum number of revolutions on one side before a trajectory must change lobes is 24. The trajectories get even more limited in the vicinity of a small number of period doubling windows. A period doubling window is a range of ρ values in which at the top of the range the steady state for the system is a simple periodic orbit, and as ρ

decreases, the system goes through a series of period doubling bifurcations where the dynamics become more and more complicated, until the system returns to a chaotic regime. There is one window near $\rho = 100$, one near $\rho = 150$, and one that starts from near $\rho = 200$ and continues for arbitrarily large ρ. At the upper end of the period doubling window between $\rho = 99.524$ and $\rho = 100.795$ there are two stable periodic orbits, each consisting of two trips around one of the stationary points and one around the other. This period doubling window is responsible for the small amplitude fluctuations shown in Figure 4.3 near $\rho = 100$. As ρ approaches the top of this period doubling window the system spends fewer orbits going around one stationary point before switching to the other, causing the average x over intermediate time to be closer to 0. At the period doubling window near $\rho = 150$ the same phenomenon happens only the stable periodic orbits at the upper end of that window are a pair of figure eights looping around each of C_1 and C_2 only once before switching lobes.

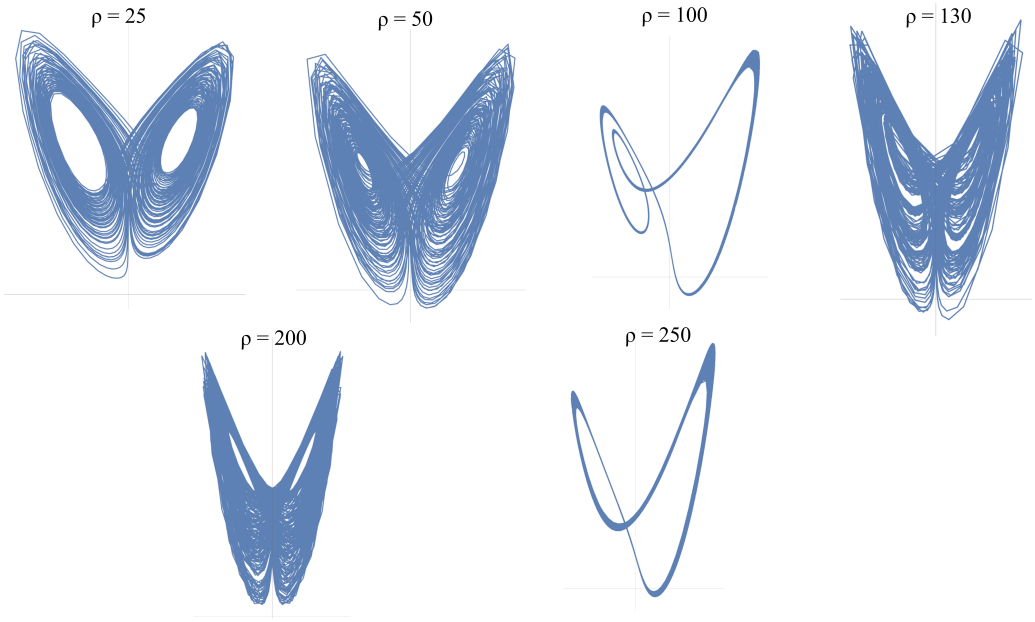

Figure 4.2: **Lorenz trajectories.** Trajectories of the Lorenz system at different values of ρ. Notice the quasi-periodic motion at $\rho = 100$ and $\rho = 250$. These are x-z projections of the full 3-dimensional system. $\sigma = 10$, $\beta = 8/3$

4.3.2 Relaxing the Parameter

Now that we have described the behavior of the standard Lorentz system, we classify ρ as the slow variable and x, y, and z as the fast variables. Clearly the behavior of x, y, and z depends on ρ already. We plan to make ρ a function of x so we first examine the flucuations in x. The average value of x over 100 time units starting from different initial conditions and different fixed values of ρ is shown in Figure 4.3. The mean of x over a long time for any one value of ρ is zero but the spread of possible x averaged over intermediate time varies. This spread plays the role of fluctuations in the force on ρ.

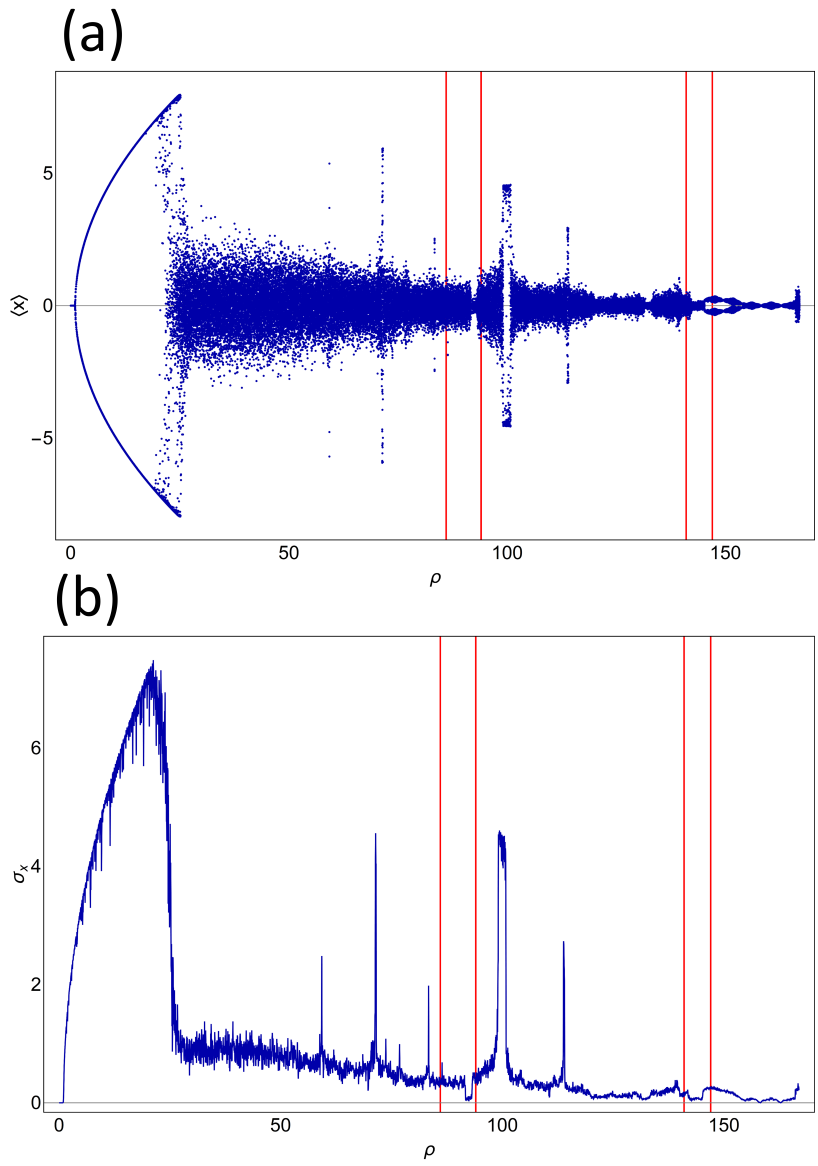

Figure 4.3: **Fluctuations in x.** The fluctuations in x in the Lorenz system from different ρ values. There are some places with very low fluctuations corresponding to period doubling windows in ρ where the trajectories become periodic. (a) A plot of the average value of x for fixed ρ over 100 time units after a short transient from random initial conditions. (b) The standard deviation of the above plot at each rho value. $\lambda = 10$

Now we let ρ vary on a time scale controlled by a constant λ.

$$\lambda\dot{\rho} = x \tag{4.10}$$

The average drift from the deterministic motion of x is zero because the average value of x is zero over long time for all values of ρ. However, the magnitude of the effective noise from x is inhomogeneous, so there is an average drift down the gradient of fluctuation amplitude toward ρ values with lower amplitude fluctuations (Highlighted in Figure 4.3).

A collection of typical trajectories of ρ is shown in Figure 4.4 where the value of ρ spends time hung up around places of low fluctuations in x before continuing to diffuse. Note that this corresponds to a regime where there are stable periodic orbits when ρ is fixed. The red lines in Figure 4.4 correspond to the same values of ρ as in Figure 4.3.

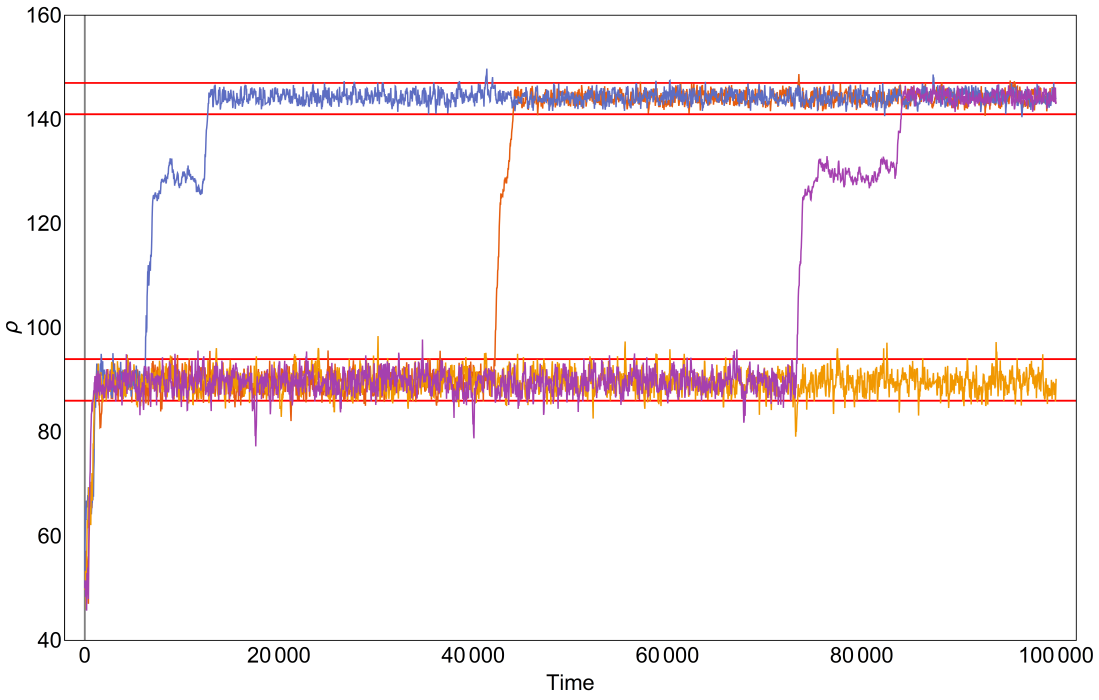

Figure 4.4: ρ **Trajectories.** A collection of ρ trajectories evolving according to Equations 4.7-4.10. The same ranges are highlighted as in Figure 4.3.

This variation of the Lorenz equations is an illustrative example of a system with many different possible behaviors parametrized by a single parameter. When this parameter is allowed to evolve as a function of the fast variables in the system, it

finds places with low fluctuations around a stationary point in its dynamical function and the diffusion slows in those places. This is an entirely deterministic system, but ρ acts qualitatively like a variable that has an average drift down a gradient of fluctuation amplitude that stalls in places of very low fluctuation amplitude until there is a large enough kick to escape those areas.

4.4 Coupled Metronomes

As an example of a many-body physical system we consider a collection of metronomes on a common moving platform. Each metronome has its own natural frequency that it will oscillate with if it is free to move on its own. A cartoon of the scenario is shown is Figure 4.5. If the platform is held stationary, the metronomes are uncoupled and the trajectory of the metronome system is a simple periodic function in the subspace of each oscillator. If we then allow the platform to move, then the metronomes are now all to all coupled with a coupling constant determined by the mass of the platform and the metronomes. In the case of strong enough coupling and close enough natural frequencies, the metronomes tend to synchronize with each other. We can understand this synchronization as follows. This system cannot find a stationary point because of the metronomes internal drive. All the possible initial conditions give rise to a collection of possible trajectories. In each one of these possible trajectories there are times when the metronomes are more synchronized and times when they are less synchronized. The forces from the coupling between the metronomes tends to pull the phases of the metronomes together because the motion of a metronome's pendulum in one direction gives a reaction force to the platform in the opposite direction that in turn gives a reaction force to all of the other pendulums to move in the same direction as the motion of the original metronome. When the metronomes are not synchronized the motion of the platform is erratic and irregular. When the metronomes are more synchronized the motion of the platform is more regular. When all the metronomes

are totally synchronized, the platform and the metronomes are following a highly regular periodic pattern. Once it finds this periodic pattern there is no way out of it without external intervention.

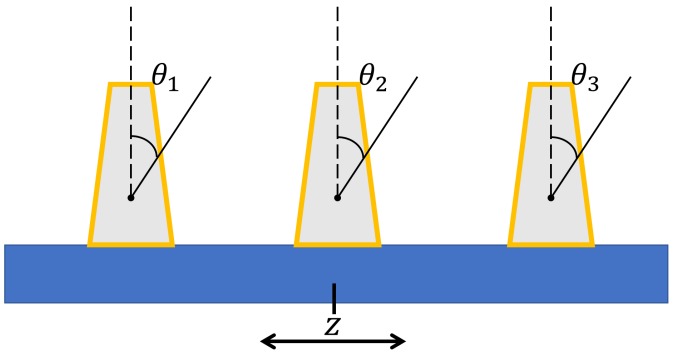

Figure 4.5: **Metronome setup.** A cartoon of the coupled metronome system. θ_i is the deflection of the pendulum of metronome i from vertical. z is the position of the platform the metronomes are sitting on.

4.4.1 Metronome System

A set of non-dimensional dynamical equations for a system of N metronomes on a platform is shown below (Equations 4.11-4.12). These equations are the same as the treatment in [60]. The θ_i are the deflections of the metronome pendulums from vertical. z is the position of the platform the metronomes are resting on. ω is the mean natural frequency of the metronomes and the ω_i are the individual natural frequencies of the metronomes. The r_i are the distances from the pivot points of the metronomes to the centers of mass of their pendulums. M is the mass of the platform and m is the mass of a pendulum. N is the number of metronomes. The difference in frequencies is created by varying the lengths r_i.

$$\ddot{\theta}_i = -\frac{\omega_i}{\omega}\sin(\theta_i) - \frac{\beta}{\omega}\left(\left(\frac{\theta_i}{\theta_0}\right)^2 - 1\right)\dot{\theta}_i - \frac{\omega_i^2}{g}\left(\frac{m}{M+Nm}\right) r_i \cos(\theta_i)\ddot{z} \tag{4.11}$$

$$\ddot{z} = -\frac{1}{r}\sum_j^N r_j \frac{\mathrm{d}^2}{\mathrm{d}t^2}\sin(\theta_j) \tag{4.12}$$

The first term for each oscillator is a simple pendulum. The second is a Van der Pol term that will give the oscillator a force in the same direction it is moving when its phase is close to zero, and give a force in the opposite direction it is moving when the phase is far from zero. This allows this term to keep the metronomes from settling while also restricting them from overturning. β controls the strength of this driving/dissipation. In the simulations shown $N = 32$, $m = .1$, $M = .5$, $\beta = .01$, $\theta_0 = \pi/16$.

4.4.2 Behavior

The behavior of the system depends on the spread of natural frequencies and the mass of the platform. When the natural frequencies are very close together and the platform is light the metronomes become synchronized, all of the phases of the metronomes move together, and the platform moves back and forth periodically with a large amplitude. When the natural frequencies are very spread apart they cannot synchronize, and they all move with their own frequencies. This causes the motion of the platform to be an erratic superposition of sinusoids. At an intermediate spread of natural frequencies the system alternates between two different behaviors. The first is one where all the metronomes are partially synchronized and the platform moves similarly to the synchronized case but with smaller amplitude. The other pattern of behavior is nearly the same as the first except the metronome with the smallest frequency falls behind the others and moves with twice the amplitude and twice the period as the rest. These different behaviors can be easily identified with

a well-chosen order parameter. Here we use the largest Fourier amplitude of the motion of the platform normalized so that the maximum possible power is 1 (Equation 4.13). This is natural because when the metronomes are unsynchronized the platform moves like the superposition of many different frequencies. When the metronomes move together, the platform moves with almost all of its power in one frequency. In practice, this means taking the discrete Fourier transform of $z(t)$ in a moving time window and taking the magnitude of the maximum amplitude over all possible frequencies in that window. A time series of this order parameter for different spreads of natural frequencies is shown in Figure 4.6.

$$O(t) = \text{Max}(\mathcal{F}[z](t)) \tag{4.13}$$

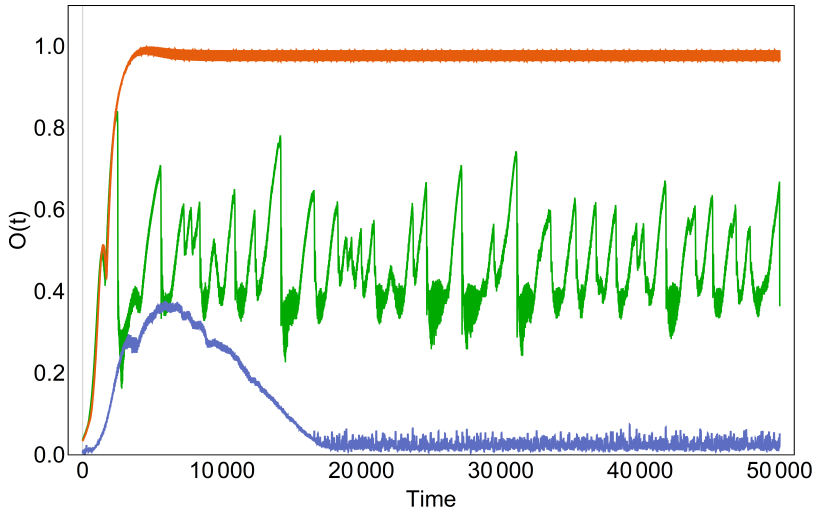

Figure 4.6: **Order Parameter.** The value of the maximum Fourier amplitude versus time for different spreads of natural frequencies. Orange corresponds to a very small spread of frequencies that allows synchrony. Blue corresponds to a very wide spread of frequencies where all of the metronomes move on their own. Green corresponds to an intermediate spread of frequencies that allows partial synchrony. Each set of frequencies is chosen by picking the arm lengths r_i from a uniform distribution within a fixed Δr about $r_i = .05$. The three Δr used here are .003, .015, and .03.

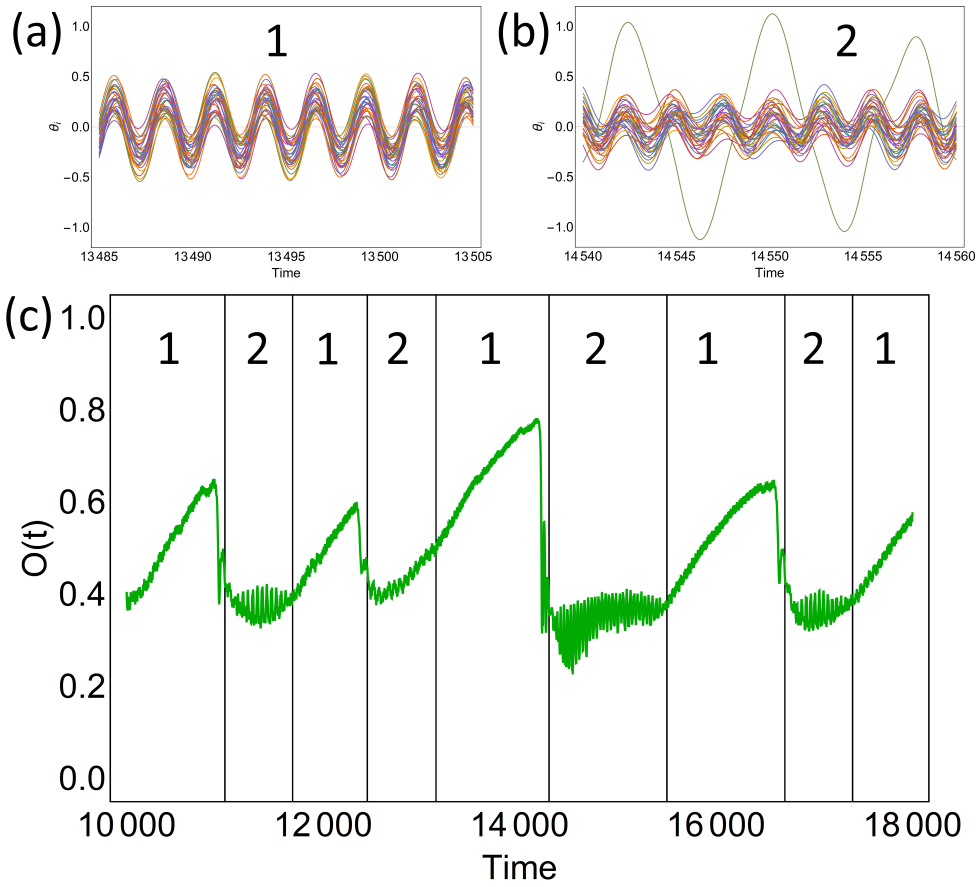

Figure 4.7: **Behavior and Parameter Detail.** A zoomed in look at the order parameter time series from Figure 4.6 with the two episodic behaviors identified. (a) Detailed look at pattern 1, where the metronomes are all moving together in a partially synchronized state. (b) Detailed look at pattern 2 where one metronome has a larger amplitude and period than the others.

The metronome systems behavior in the intermediate regime is qualitatively similar to the double well system shown in Figure 4.1(a). There are two different behaviors that the system can exhibit from a dynamical point of view. The system switches between these two behaviors episodically after irregular time intervals. The difference is that there is no explicit driving noise that can kick the system from one state to another. However, there are still fluctuations in the system because of the disorder in natural frequencies of the oscillators. Because the frequencies of the oscillators are too spread out for them to exactly phase lock with each other, the motion of the

platform is irregular, and this causes an effective noise in the dynamics similar to the Lorenz system in Section 4.3.2. It is this noise that kicks the system back and forth between two patterns of behavior.

4.5 Discussion

We have described a class of system where the dynamics are a combination of dynamical deterministic forces and noisy fluctuations. The signature of this type of system is the exhibition of episodes of distinct behavior with irregular transitions between them. The simple picture is some number of attractors that persist from the deterministic forces and strong enough noise to kick the system from one attractor to another, but not so strong that the original attractors are washed out. The fluctuations need not be from explicit noise driving the system but can also come from the complicated dynamics of a chaotic or a quickly varying subset of the elements in the system.

4.5.1 Relation to Adaptive Control

The slow drift of parameters to low noise amplitude places in parameter space bears some resemblance to the structure of adaptive control in so called self-tuning regulators [61]. This type of regulator is a scheme for controlling the output of a system with slowly varying and/or uncertain parameter values. For example, this kind of controller can be used in flight navigation controllers to adapt to external disturbances or the change in airplane mass from the burning of fuel [62]. The scheme involves first developing a reference model for the input and output of the system. Then parameter values are given an initial estimate. Then a desirable series of outputs for the system is prepared. An external control signal is applied to the system with the goal of minimizing the error between the actual output of the system and the desired output [63, 64]. Adaptive control relies on a mathematical model for the

system in question and on the estimation of parameter values within that model. The response of the system to an injected control signal changes depending on these parameter values and so the control signal is also changed in turn to produce the desired output.

The theories presented in this chapter also rely on the parameters of a system changing and in turn change the behavior of the system. The system can also prefer a particular behavior in the space of behaviors allowed by its parameter space. A major difference between the adaptive control paradigm and fluctuation feedback is that in adaptive control the preferred behavior of the system is preselected by a systems engineer to achieve a particular goal. The drift of parameter values is taken as a given background and a behavior is forced with a control signal. In the theory presented in this chapter, and particularly in the modified Lorenz system, a behavior of the system in chosen autonomously by the reduction in fluctuations in the fast variables. The framework presented here may have some application in the estimation of parameter values in a system given a preference for low fluctuation states but otherwise fluctuation feedback and adaptive control are quite separate. The drift of parameter values is only a small part of adaptive control schemes which can include parameter estimation and drift, modeling assumptions, mapping of internal and external degrees of freedom, and control signaling with open or closed loop feedback.

4.5.2 Examples for Possible Application

One place where this class of system could arise is in a supersmarticle system similar to the one discussed in Chapter 3. In experiments where a small number of smarticles are placed in an anchored ring they quickly find nearly periodic patterns where the same series of collisions between the smarticles and the ring will happen repeatedly for some time before the pattern breaks up again [65]. Some of these patterns are clear to the eye and upon further study, a small collection of five to six

of them are identifiable. An extended experiment shows multiple of these patterns in succession even within the same experimental run. The question arises, why are these patterns so prevalent in a system that at times seems very nonlinear and quasi-stochastic. The answer could lie in the simple fact that these patterns are nearly periodic, so the fluctuations are low, and the system comes back to almost the same configuration it was in one period of the smarticle gate ago. This means that in any one of these nearly periodic patterns, once the system falls into one it will on average take a long time to leave so the average time in a pattern is extended. The time in between patterns is short because this time consists of configurations that change drastically after a smarticle gate period.

Another possible example of this class of system is evolutionary punctuated equilibrium [66, 67]. This theory contends that the reason we do not find "infinitely numerous transitional links" as Darwin put it [68] is that speciation mostly acts in rapid spurts with long episodes of little morphological change in-between. This is opposed to a model of consistent slow species change over geological time. These claims are supported by the fact that the paleolithic record is dominated by stasis rather than change [69]. This could be because once a species finds a morphological state that is adapted to the external pressures it experiences, strong deviations from the mean are mostly unfavorable, so it takes a mutation in a rare favorable direction to increase the fitness of an organism. This would lead to the organisms in a stable species to exist close to the morphological mean by culling almost all members with large mutations. This would mean low fluctuations in morphology until there is an extreme change in its environment or a large enough mutation to find another stable state. Support of this connection to evolutionary selection can be found in the Bak-Sneppen model [70]. In this simple model of selection, we start with a one dimensional array of members with periodic boundary conditions. We then assign each member a random number between 0 to 1 known as its fitness. To evolve the system, we follow

the simple rule of picking out the member with the lowest fitness and replacing that member and its immediate neighbors by re-rolling their values. The system reaches a state where the all of the fitnesses are above a critical threshold. We can then define an "avalanche" as a series of replacements where some fitness is less than that threshold. The distribution of avalanche sizes in time have the form $P(s) \propto s^{-\tau}$ with critical exponent τ. In this state small avalanches are much more likely than large ones, but all sizes of avalanches are possible. This leads to the fitness configuration of the system changing slowly through small avalanche events almost all the time until, every once in a while, there is a system wide event that rearranges the entire system configuration. This is an example of a system that starts with a random initial condition and quickly finds a steady state where the fluctuations are small in general, but there is still the occasional kick that pushes the system as a whole into a different steady state configuration. The above connection between the episodic behavior described in this chapter, punctuated equilibrium, and the self-organized criticality of the Bak-Sneppen model is speculative and phenomenological in nature, but all three concepts seem to arise in many-body systems where there is a competition between ordered and disordered behavior.

4.6 Summary

In this chapter we have examined the validity of some very general claims made in [3] about the behavior of non-equilibrium, many body systems through a small number of concrete examples. Through these examples we have shown that it can be useful and instructive to approximate the complicated internal dynamics of a system with noise. We have also described a way to understand episodic behavior in a subclass of these systems. We showed that if the noise amplitude is low enough not to destroy those states, but still high enough to kick the system over the barrier between them, the result is a behavior where the system switches between the possible final states

episodically. We also showed that if the noise landscape is inhomogeneous between the final states, then the system will prefer the state with the lower amplitude noise.

Bibliography

[1]P. A. Tass, I Adamchic, H. J. Freund, T Stackelberg, and C Hauptmann, "Counteracting tinnitus by acoustic coordinated reset neuromodulation (German)", Restorative Neurology and Neuroscience **30**, 137–159 (2012).

[2]W Savoie, T. A. Berrueta, Z Jackson, A Pervan, R Warkentin, S Li, T. D. Murphey, K Wiesenfeld, and D. I. Goldman, "A robot made of robots: emergent transport and control of a smarticle ensemble", Science Robotics **4**, eaax4316 (2019).

[3]P. Chvykov, and J. England, "Least-rattling feedback from strong time-scale seperation", Physical Review E **97**, 032115 (2018).

[4]G. Longo, M. Montévil, and A. Pocheville, "From bottom-up approaches to levels of organization and extended critical transitions", Frontiers in Physiology **3** (2012).

[5]J. P. Sethna, *Entropy, order parameters, and complexity* (Clarendon Press, Oxford, 2017).

[6]K. G. Wilson, "Renormalization group and critical phenomena. i. renormalization group and the kadanoff scaling picture", Phys. Rev. B **4**, 3174–3183 (1971).

[7]K. G. Wilson, "Renormalization group and critical phenomena. ii. phase-space cell analysis of critical behavior", Phys. Rev. B **4**, 3184–3205 (1971).

[8]L. D. Landau, "On the theory of phase transitions (translated to English)", Zh. Eksp. Teor. Fiz **1**, 19–32.

[9]M. Morse, and G. A. Hedlund, "Symbolic dynamics", American Journal of Mathematics **60**, 815–866 (1938).

[10]S. Strogatz, *Nonlinear dynamics and chaos: with applications to physics, biology, chemistry, and engineering (studies in nonlinearity)* (Westview Press, 2001).

[11]Y Kuramoto, "Lecture notes in physics, international symposium on mathematical problems in theoretical physics", **39**, 420 (1975).

[12]D Cumin, and C. P. Unsworth, "Generalising the kuromoto model for the study of neuronal synchronisation in the brain", Physica D **226**, 181–196 (2007).

[13]M Breakspear, S Heitmann, and A Daffertshofer, "Generative models of cortical oscillations: neurobiological implications of the kuramoto model", Front Hum Neurosci **4** (2010).

[14]S. Strogatz, *Sync: the emerging science of spontaneous order* (Hyperion, New York, 2003).

[15]K. Wiesenfeld, P. Colet, and S. H. Strogatz, "Frequency locking in josephson arrays: connection with the kuramoto model", Phys. Rev. E **57**, 1563 (1998).

[16]B. C. Daniels, S. T. M. Dissanayake, and B. R. Trees, "Synchronization of coupledrotators: josephson junction ladders and the locally coupled kuramoto model", Phys. Rev. E **67**, 026216 (2003).

[17]S. Strogatz, "Norbert wiener's brain waves", in *Frontiers in mathematical biology: lecture notes in biomathematics*, edited by S. A. Levin, (Springer, Berlin, 1994), pp. 122–138.

[18]J Bélair, L Glass, U Heiden, and J Milton, "Dynamical disease: identification, temporal aspects and treatment strategies of human illness", Chaos **5**, 1–7 (1995).

[19]L. Glass, "Dynamical disease: challenges for nonlinear dynamics and medicine", Chaos: An Interdisciplinary Journal of Nonlinear Science **25**, 097603 (2015).

[20]M. Mackey, and L Glass, "Oscillation and chaos in physiological control systems", Science **197**, 287–289 (1977).

[21]L. Glass, and M. C. Mackey, "Pathological conditions resulting from instabilities in physiological control systems*", Annals of the New York Academy of Sciences **316**, 214–235 (1979).

[22]I. M. Held, and M. J. Suarez, "Simple albedo feedback models of the icecaps", Tellus **26**, 613–629 (1974).

[23]B Nadrowski, P Martin, F Jülicher, and A. J. Hudspeth, "Active hair-bundle motility harnesses noise to operate near an optimum of mechanosensitivity", Proceedings of the National Academy of Sciences of the United States of America **101**, 12195–12200 (2004).

[24]D Baguley, D McFerran, and D Hall, "Tinnitus", Lancet **382**, 1600–16007 (2013).

[25]H. J. Hoffman, and G Reed, "Epidemiology of tinnitus", in *Tinnitus: theory and managment*, edited by J. B. Snow, (BC Decker Inc, Hamilton, 2004) Chap. 3, pp. 16–41.

[26]P Adjamiana, M Seredaa, and D. A. Hallab, "The mechanisms of tinnitus: perspectives from human functional neuroimaging", Hearing Research **253**, 15–31 (2009).

[27]P. A. Tass, and O. V. Popovych, "Unlearning tinnitus-related cerebral sychrony with acoustic coordinated reset stimulation: theoretical concept and modeling", Biological Cybernetics **106**, 27–36 (2012).

[28]J. J. Eggermont, and P. A. Tass, "Maladaptive neural synchrony in tinnitus: origin and restoration", Front. Neural **6**, 29 (2015).

[29]S Seki, and J. J. Eggermont, "Changes in spontaneous firing rate and neural sychrony in cat primary sudio cortex after localized tone-induced hearing loss", Hear Res. **180**, 28–38 (2003).

[30]A. J. Norena, and J. J. Eggermont, "Changes in spontaneous neural activity immediately after an acoustic trauma: implications for neural correlates of tinnitus", Hear Res. **183**, 137–153 (2003).

[31]P. A. Tass, "A model of desychronizing deep brain stimulation with a demand-controlled coordinated reset of neural subpopulations", Biological Cybernetics **89**, 81–88 (2002).

[32]A. J. Hudspeth, F. Jülicher, and P. Martin, "A critique of the critical cochlea: Hopf—a bifurcation—is better than none", Journal of Neurophysiology **104**, PMID: 20538769, 1219–1229 (2010).

[33]O. V. Popovych, B Lysyansky, M Rosenblum, A Pikovsky, and P. A. Tass, "Pulsatile desynchronizing delayed feedback for closed-loop deep brain stimulation", PLoS ONE **12**, (e0173363 (2017).

[34]M Ospeck, V. M. Eguiluz, and M. O. Magnasco, "Evidence of a hopf bifrurcation in frog cells", Biophysical Journal **80**, 2597–2607 (2001).

[35]S Camalet, T Duke, F Jülicher, and J Prost, "Auditory sensitivity provided by self-tuned critical oscillations of hair cells", PNAS **97**, 3183–3188 (2000).

[36]T Mora, and W Bialek, "Are biological systems poised at criticality?", J Stat Phys **144**, 268–302 (2011).

[37]D. R. Trune, "Ion homeostasis in the ear: mechanisms, maladies, and management", Curr Opin Otollaryngol Head Neck Surg **18**, 412–419 (2010).

[38]G Tkacik, E Schneidman, M. J. Berry II, and W Bialek, "Ising models for networks of real neurons", arXiv:q-bio.NC (2006).

[39]K. M. Garza, L. Zhang, B. Borron, L. B. Wood, and A. C. Singer, "Gamma visual stimulation induces a neuroimmune signaling profile distinct from acute neuroinflammation", The Journal of Neuroscience **40**, 1211–1225 (2020).

[40]L. E. Parker, "Alliance: an architecture for fault tolerant multirobot cooperation", IEEE Transactions on Robotics and Automation **14**, 220–240 (1998).

[41]W. J. Reichmann, *The use and abuse of statistics* (Oxford University Press, New York, 1961).

[42]C. M. Grinstead, and L. J. Snell, *Introduction to probability* (American Mathematical Society, Providence, 1997).

[43]M. Brambilla, E. Ferrante, M. Brittari, and M. Dorigo, "Swarm robotics: a review from the swarm engineering perspective", Swarm Intell **7**, 1–41 (2013).

[44]F. Arvin, J. Murray, L. Shi, C. Zhang, and S. Yue, "Development of an autonomous micro robot for swarm robotics", in (Aug. 2014), pp. 635–640.

[45]M. M. Stanton, B.-W. Park, A. Miguel-López, X. Ma, M. Sitti, and S. Sánchez, "Biohybrid microtube swimmers driven by single captured bacteria", Small **13**, 1603679 (2017).

[46]K. Y. Wan, and R. E. Goldstein, "Coordinated beating of algal flagella is mediated by basal coupling", Proceedings of the National Academy of Sciences **113**, E2784–E2793 (2016).

[47]T. Nakagaki, "Smart behavior of true slime mold in a labyrinth", Research in Microbiology **152**, 767 –770 (2001).

[48]C. R. Kube, and E. Bonabeau, "Cooperative transport by ants and robots", Robotics and Autonomous Systems **30**, 85–101 (2000).

[49]G. Vásárhelyi, C. Virágh, G. Somorjai, T. Nepusz, A. E. Eiben, and T. Vicsek, "Optimized flocking of autonomous drones in confined environments", Science Robotics **3** (2018) 10.1126/scirobotics.aat3536.

[50]L. Iocchi, D. Nardi, and M. Salerno, "Reactivity and deliberation: a survey on multi-robot systems", in *Balancing reactivity and social deliberation in multi-agent systems*, edited by M. Hannebauer, J. Wendler, and E. Pagello, (Springer, Berlin, Heidelberg, 2001), pp. 9–32.

[51]K. Y. Wan, and R. E. Goldstein, "Coordinated beating of algal flagella is mediated by basal coupling", Proceedings of the National Academy of Sciences **113**, E2784–E2793 (2016).

[52]T. Balch, "The impact of diversity on performance in multi-robot foraging", in Proceedings of the third annual conference on autonomous agents, AGENTS '99 (1999), 92–99.

[53]D. Jung, and A. Zelinsky, "Grounded symbolic communication between heterogeneous cooperating robots", Autonomous Robots **8**, 269–292 (2000).

[54]L. E. Parker, "Lifelong adaptation in heterogeneous multi-robot teams: response to continual variation in individual robot performance", Autonomous Robots **8**, 239–267 (2000).

[55]N. Gravish, S. V. Franklin, D. L. Hu, and D. I. Goldman, "Entangled granular media", Phys. Rev. Lett. **108**, 208001 (2012).

[56]R. Maiocchi, "The case of brownian motion", The British Journal for the History of Science **23**, 257–283 (1990).

[57]B. Eckhardt, and D. Yao, "Local lyapunov exponents in chaotic systems", Physica D: Nonlinear Phenomena **65**, 100 –108 (1993).

[58]E. N. Lorenz, "Deterministic nonperiodic flow", Journal of the Atmospheric Sciences **20**, 130–141 (1963).

[59]C. Sparrow, *The lorenz equations: bifrications, chaos, and strange attractors* (Springer-Verlag, New York, 1982).

[60]H. Ulrichs, A. Mann, and U. Parlitz, "Sychronization and chaotic dynamics of coupled mechanical metronomes", Chaos **19**, 043120 (2009).

[61]K. Åström, and B. Wittenmark, "On self tuning regulators", Automatica **9**, 185 –199 (1973).

[62]S. K. Kannan, G. V. Chowdhary, and E. N. Johnson, "Adaptive control of unmanned aerial vehicles: theory and flight tests", in *Handbook of unmanned aerial vehicles*, edited by K. P. Valavanis, and G. J. Vachtsevanos, (Springer Netherlands, Dordrecht, 2015), pp. 613–673.

[63]G. Tao, "Multivariable adaptive control: a survey", Automatica **50**, 2737 –2764 (2014).

[64]E. Lavretsky, "Robust and adaptive control methods for aerial vehicles", in *Handbook of unmanned aerial vehicles*, edited by K. P. Valavanis, and G. J. Vachtsevanos, (Springer Netherlands, Dordrecht, 2015), pp. 675–710.

[65]P. Chvykov, "On typicality and adaptation in driven dynamical systems", PhD thesis (Massachusetts Institute of Technology, MIT Libraries, May 2019).

[66]N Eldredge, and S. J. Gould, "Punctuated equilibria: an alternative to phyletic gradualism", in *Models in paleobiology*, edited by T. Schopf, (Freeman Cooper, San Francisco, 1972) Chap. 5, pp. 82–115.

[67]S. J. Gould, and N Eldredge, "Punctuated equilibria: the tempo and mode of evolution reconsidered", Paleobiology **3**, 115–151 (1977).

[68]C. R. Darwin, *On the origin of species by means of natural selection, or the preservation of favoured races in the struggle for life* (John Murray, London, 1859).

[69]M. J. Benton, and P. N. Pearson, "Speciation in the fossil record", TRENDS in Ecology & Evolution **16**, 5209–5213 (2001).

[70]P Bak, and K Sneppen, "Punctuated equilibrium and criticality in a simple model of evolution", Physical Review Letters **71**, (24):4083–4086 (1993).